Spontaneous Stratospheric QBO-like Oscillations Simulated by the GFDL SKYHI General Circulation Model

KEVIN HAMILTON

Department of Meteorology and International Pacific Research Center, University of Hawaii at Manoa, Honolulu, Hawaii

R. JOHN WILSON AND RICHARD S. HEMLER

NOAA/Geophysical Fluid Dynamics Laboratory, Princeton, New Jersey

(Manuscript received 17 October 2000, in final form 30 March 2001)

ABSTRACT

The tropical stratospheric mean flow behavior in a series of integrations with high vertical resolution versions of the Geophysical Fluid Dynamics Laboratory (GFDL) ''SKYHI'' model is examined. At sufficiently high vertical and horizontal model resolution, the simulated stratospheric zonal winds exhibit a strong equatorially centered oscillation with downward propagation of the wind reversals and with formation of strong vertical shear layers. This appears to be a spontaneous internally generated oscillation and closely resembles the observed quasi-biennial oscillation (QBO) in many respects, although the simulated oscillation has a period less than half that of the real QBO. The same basic mean flow oscillation appears in both seasonally varying and perpetual equinox versions of the model, and most of the analysis in this paper is focused on the perpetual equinox cases. The mean flow oscillation is shown to be largely driven by eddy momentum fluxes associated with a broad spectrum of vertically propagating waves generated spontaneously in the tropical troposphere of the model. Several experiments are performed with the model parameters perturbed in various ways. The period of the simulated tropical stratospheric mean flow oscillation is found to change in response to large alterations in the sea surface temperatures (SSTs) employed. This is a fairly direct demonstration of the link between the stratospheric mean flow behavior and tropical convection that is inherent in current theories of the QBO. It is also shown in another series of experiments that the oscillation is affected by the coefficients used for the subgrid-scale diffusion parameterization. These experiments demonstrate that at least one key reason why reasonably fine horizontal resolution is needed for the model to simulate a mean flow oscillation is the smaller horizontal diffusion that can be used at high resolution.

1. Introduction

The ability of comprehensive general circulation models (GCMs) to simulate the quasi-biennial oscillation (QBO) of the tropical stratosphere has been a concern for over three decades. The earliest GCMs with numerical levels in the stratosphere (Manabe and Hunt 1968; Kasahara and Sasamori 1974; Manabe and Mahlman 1976) all simulated mean winds in the equatorial region that were very steady, and the absence of a QBO was immediately understood as a major failing in these models. These early GCM experiments coincided with the key developments in the theory of the QBO. In particular, the crucial role of mean momentum transport by vertically propagating waves was convincingly established (Lindzen and Holton 1968; Holton and Lindzen 1972; Plumb 1977; Plumb and McEwan 1978). These theoretical developments helped guide analysis of GCM results in the tropical stratosphere (Hayashi 1974; Tsay 1974) and they provided speculation on the cause of the poor representation of the tropical stratospheric mean winds in GCMs (e.g., Plumb 1984).

The first promising hint that GCMs might be able to reproduce QBO-like mean wind behavior came in the work of Mahlman and Sinclair (1980). They reported on integrations with two versions of the Geophysical Fluid Dynamics Laboratory (GFDL) ''SKYHI'' GCM (Fels et al. 1980), a GCM with then-unprecedented vertical resolution in the middle atmosphere (40 levels between the ground and 0.01 hPa). Their initial integration employed a version with 9° lat × 10° long grid resolution, and this produced very steady winds in the equatorial stratosphere (although these were westerly winds rather than easterlies as found in earlier GCMs). After several months of running this version, the fields from an instantaneous snapshot of the results were interpolated onto a 5° × 6° grid and this was used as the initial condition for a higher-resolution version of the model.

Corresponding author address: Dr. Kevin Hamilton, Department of Meteorology and International Pacific Research Center, University of Hawaii at Manoa, Honolulu, HI 96822.
E-mail: kph@soest.hawaii.edu

The equatorial mean winds immediately began accelerating from westerlies toward easterlies throughout the entire middle atmosphere, with the peak accelerations appearing initially at high altitudes and propagating downward. This downward vertical phase propagation is a distinctive feature of the observed QBO and is an expected consequence of the interaction of the mean flow with dissipating vertically propagating waves (Lindzen and Holton 1968; Holton and Lindzen 1972). However, the tropical winds in this early SKYHI model stabilized after a few months and no actual oscillation occurred.

The number of GCMs including a serious representation of the middle atmosphere grew during the 1980s and 1990s, and today there are about a dozen such models (e.g., Hamilton 1996; Pawson et al. 2000). These models are typically run with ~1.5–3 km vertical level spacing in the stratosphere. Until very recently, standard control integrations with available models had mean winds in the tropical stratosphere with very little interannual variability (at most a few m s^{-1}; see Cariolle et al. 1993; Hamilton et al. 1995). Hamilton and Yuan (1992) conducted some experiments in which the equatorial stratospheric mean winds in a spectral GCM were instantaneously perturbed. The subsequent relaxation of the tropical mean winds was found to resemble the downward-propagating QBO wind reversals, at least in terms of peak acceleration and downward phase propagation. This suggests that the current GCMs may have a reasonable representation of the wave–mean flow dynamics thought to be important in the QBO, even if the they still have some deficiency that prevents spontaneous simulation of the complete QBO cycle. A similar conclusion was reached by Hamilton (1998), who imposed a realistic QBO on the tropical mean winds in a version of the SKYHI model and analyzed the detailed zonal-mean momentum balance.

The first demonstration that GCMs could spontaneously produce a large-amplitude interannual oscillation in the stratospheric winds was in the work of Takahashi (1996). He ran a triangular-21 version of the Japanese Center for Climate System Research (CCSR) spectral GCM, but with several changes from its usual formulation when employed in climate studies. In particular, the vertical resolution was enhanced to be about 0.5 km in the stratosphere, the standard moist convection scheme was replaced with moist convective adjustment, and the coefficient of the horizontal hyperdiffusion was reduced by a factor of 10 from the standard value. With these changes the model simulated a fairly regular oscillation in the equatorial zonal-mean zonal wind from strong easterlies to strong westerlies throughout the middle and upper stratosphere. In terms of peak amplitude and phase progression the model oscillation agreed well with the QBO, but it had a period of only ~1.4 yr and was centered unrealistically high in the atmosphere, with very weak amplitude in the lower stratosphere (particularly below ~25 km). Horinouchi and Yoden (1998) found a similar oscillation in a fine vertical resolution version of another spectral GCM run in a simplified ''aquaplanet'' mode (all ocean surface and no zonal variations in SSTs). Takahashi (1996) coined the term ''QBO-like oscillation'' (QLO) to describe the equatorial mean flow behavior they saw—namely, spontaneous, large-amplitude mean wind oscillations with downward-propagating shear zones, although with a period substantially different from that of the real QBO and possibly with a somewhat different vertical amplitude modulation than the real QBO. Untch (1998) found a roughly biennial oscillation in the tropical mean flow in fine vertical resolution versions of the European Centre for Medium-Range Weather Forecasts (ECMWF) spectral model. Interestingly, Untch found that in the triangular-63 horizontal resolution version of her model, the oscillation persisted for a few cycles then spontaneously disappeared. The model described recently by Takahashi (1999), with increased horizontal resolution and further reduced subgrid-scale mixing, also produces a tropical mean flow oscillation with realistic QBO period.

A spontaneous QLO was recently found in integrations of the GFDL SKYHI troposphere–stratosphere–mesosphere GCM when run at sufficiently high vertical and horizontal model resolution. This basic result in the control experiment was reported briefly in Hamilton et al. (1999, hereafter HWH). The present paper will provide a detailed analysis of this oscillation in the model reported in HWH and, more particularly, in some more extensive control and perturbed experiments conducted with a somewhat coarser horizontal resolution version of SKYHI. The paper is structured as follows. Section 2 reviews some basic theory for the QBO, which will be useful background for the interpretation of the present GCM experiments. Section 3 briefly describes the SKYHI model. Section 4 presents the basic results for the tropical stratospheric winds in SKYHI control integrations at both high and moderate horizontal resolution. Section 5 describes a more detailed analysis of the dynamics involved in the mean flow oscillation in the moderate horizontal resolution control runs. Section 6 presents results from a suite of additional experiments with the moderate horizontal resolution model, but with modifications to the subgrid-scale closure schemes and to the prescribed ocean surface temperatures. The conclusions are summarized in section 7.

2. Background

The most successful theories of the dynamics of the QBO invoke the interaction of vertically propagating waves with the mean flow (Lindzen and Holton 1968; Holton and Lindzen 1972). Perhaps the simplest prototype of this process is provided by the one-wave model of Plumb (1977) in which an internal gravity wave interacts with a mean flow that depends only on height. When the problem is further simplified by assuming

linearity, quasi-steadiness, a mean flow that varies slowly in the vertical relative to the wave phase variations, linear wave damping, planar geometry, and no rotation, then the Reynolds stress associated with the wave can be written as

$$F(z) = F(z_o) \exp\left(- \int_{z_o}^{z} \frac{\alpha}{W_g} \, dz \right), \tag{1}$$

where z is the height, $\alpha(z)$ is the wave dissipation coefficient, and W_g is the vertical group velocity that is given by

$$W_g = \frac{k(c - \overline{u})^2}{N}, \tag{2}$$

where k is the horizontal wavenumber, $\overline{u}(z)$ is the mean flow, c is the horizontal phase speed, and $N(z)$ is the Brunt–Väisälä frequency. The contribution to the mean flow acceleration from the wave is then

$$-\frac{1}{\rho_o} \frac{\partial F}{\partial z}, \tag{3}$$

where $\rho_0(z)$ is the mean density. One interesting limit is that for small-scale waves (large k) and weak wave dissipation. In this limit, the group velocity is large everywhere except very close to critical levels where $\overline{u} = c$. In this case, the total wave flux will be absorbed near the critical level. When generalized to a continuous spectrum of waves, this leads to a mean flow forcing that is proportional to the local shear of the mean flow (Lindzen and Holton 1968; Dunkerton 1997). This provides a mechanism to maintain and propagate any preexisting mean flow shears, although not to initiate such shears (Lindzen and Holton 1968). Waves with large horizontal scale have smaller group velocity and can be significantly absorbed even in the absence of critical levels (Lindzen 1971). When a simple prognostic model of the mean flow is forced with wave fluxes parameterized by Eq. (1), a long-period mean flow oscillation can result, provided that the wave spectrum assumed has significant flux in both eastward- and westward-propagating directions. Lindzen and Holton (1968) showed that a long-period mean flow oscillation could result from the critical level interaction of the mean flow with a continuous spectrum of small-scale gravity waves, while Holton and Lindzen (1972) demonstrated that a similar result could be obtained by including only a limited discrete spectrum of planetary-scale waves and allowing radiative cooling to act to damp the waves. The relative roles of small-scale and planetary-scale waves in the real QBO is still a matter of investigation (e.g., Dunkerton 1997; Sato and Dunkerton 1997).

Another interesting feature of the simple QBO models is the scaling of the simulated mean flow period as a function of the imposed wave properties. In simple models forced by two waves with opposite phase speed, Plumb (1977) showed that including stronger waves leads to a shorter-period mean flow oscillation. This result will be the motivation for some of the SKYHI GCM experiments reported in section 6 in which the tropospheric forcing of vertically propagating waves was modified (by changing the prescribed ocean temperatures) with interesting effects on the tropical stratospheric mean wind evolution.

Finally the results in Plumb (1977) concerning the role of mean flow dissipation in simple QBO models should be noted. In the one-dimensional QBO models of Holton and Lindzen (1972) and Plumb (1977), it is necessary to include a vertical mean flow diffusivity. Plumb found that raising the value of the diffusivity coefficient to a sufficiently high value completely suppresses the mean flow oscillation in his simple model. Plumb (1984) speculated that the relatively large values of horizontal diffusivity employed in GCMs could, by analogy, be responsible for preventing simulation of the QBO. Some SKYHI experiments to be discussed in section 6 confirm that this speculation does explain the absence of the tropical mean flow oscillations in low horizontal resolution versions of SKYHI.

3. The SKYHI model formulation

The SKYHI model (Fels et al. 1980; Hamilton et al. 1995) solves the primitive equations on a latitude–longitude nonstaggered grid using second-order horizontal differencing. The model uses a hybrid vertical coordinate that is terrain following near the ground, merging into pure isobaric coordinates above 353 mb. The various latitude–longitude resolutions referred to in this paper are denoted N30 (3°–3.6°), N45 (2°–2.4°), N90 (1°–1.2°), and N270 (0.33°–0.4°), where the N notation refers to the number of grid rows between the pole and equator. The different vertical resolutions discussed are L40 and L80, where the notation gives the number of full model levels between the ground and 0.01 hPa (~80 km). The distribution of levels for the L80 grid is shown on the axis of Fig. 1. The L40 grid represents a nearly uniform doubling in level spacing throughout the domain (see HWH).

Radiative calculations and parameterizations of the interactions with the surface are discussed in Hamilton et al. (1995) and HWH. In the present control integrations, the surface temperatures at ocean points are prescribed with realistic, seasonally varying, climatological values (Hamilton et al. 1995). The model includes a standard moist convective adjustment scheme as well as a simple parameterization of precipitation in convectively stable but saturated conditions.

No parameterization of subgrid-scale gravity wave effects is included in any of the model integrations discussed here. The vertical and horizontal subgrid-scale diffusion of heat and momentum are parameterized with second-order diffusion with coefficients that depend on the vertical and horizontal grid spacing, respectively. The expression for the coefficient of the vertical dif-

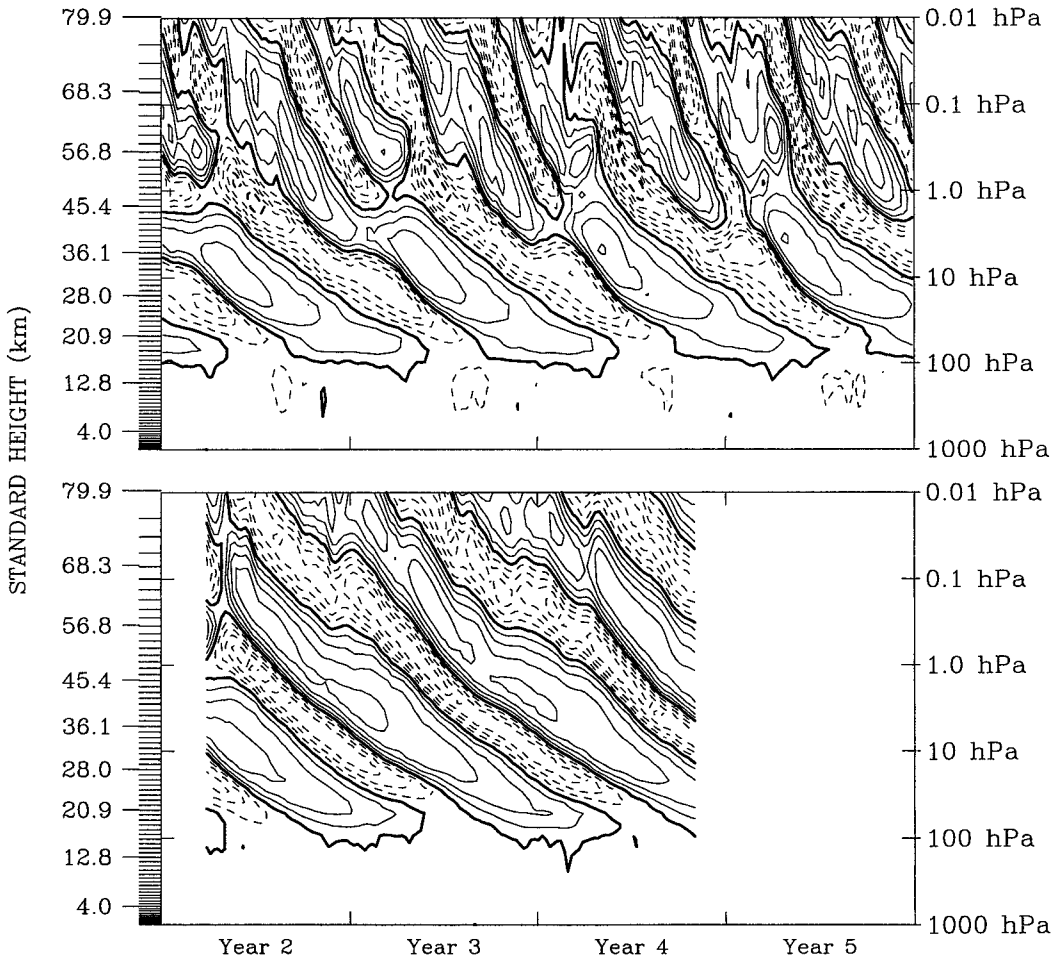

FIG. 1. The height–time section of the equatorial zonal-mean zonal wind in (top) the seasonally varying N90L80 control run and (bottom) the perpetual equinox N90L80 run. The locations of the model levels are shown by the tick marks on the axis. The pressure levels given on the right axis are for the midlatitude spring–fall U.S. Standard Atmosphere. The contour interval is 10 m s^{-1} and easterlies are denoted by dashed contours. The heavy solid contour denotes zero mean wind.

fusivity of horizontal momentum is (Levy et al. 1982)

$$K_v = K_m \quad \text{if Ri} > A/4 \tag{4}$$

$$K_v = K_m + l^2 S(1 - 4\text{Ri}/A)^{0.5} \quad \text{if } 0 < \text{Ri} < A/4 \tag{5}$$

$$K_v = K_m + l^2 S \quad \text{if Ri} < 0, \tag{6}$$

where K_m is the molecular viscosity (negligible in the height range of present interest), l is the mixing length (taken to be a constant 30 m), S is the magnitude of the vertical shear, and Ri is the Richardson number of the explicitly resolved flow. The factor A is designed to account for the subgrid-scale inhomogeneity in the vertical shear and is taken to be

$$A = 1 + 0.1(10\Delta z)^{1.5}, \tag{7}$$

where Δz is the spacing between adjacent layers in km. This factor approaches unity when the level spacing becomes small, and allows instability at larger resolved Ri when the level spacing is large. The coefficient of horizontal diffusivity depends on the local horizontal deformation field and is scaled as the square of the horizontal grid spacing [see Andrews et al. (1983) for details].

4. The control experiments and basic results

Hamilton et al. (1995) reported on multiyear control integrations with N30L40, N45L40, and N90L40 versions of the SKYHI GCM, and none of these models showed significant interannual variability of the equatorial stratospheric mean winds. A control integration with the N90L80 version was described in HWH and has since been continued for several more years. This is a seasonally varying run that was initialized from a snapshot on 5 May from the middle of an earlier N90L40 control run. As noted in HWH, this model produced a strong equatorial mean flow oscillation with properties

similar to that of the QBO, notably downward propagation of strong shear zones, but with a period that appeared to be exactly 1 yr. Figure 1 (top) shows the height–time section of equatorial $\overline{u}$ for years 2–5 of this integration (extending the record presented in Fig. 14b in HWH). The strong annual period oscillation is evident. In order to see whether the annual cycle was the key forcing for this oscillation, HWH reported as well on a simulation with perpetual equinox (PE) radiative forcing and SSTs. This was initialized from 22 March of year 2 of the N90L80 seasonal control run and produced a very similar oscillation in the equatorial winds. Figure 1 (bottom) shows the equatorial $\overline{u}$ from this run, now available for 32 months (extending Fig. 14c of HWH). The strong semiannual oscillation in the mesosphere apparent in the seasonal run is completely absent in the PE run, but the stratospheric mean wind oscillation is quite similar in the two model integrations. The period of the oscillation in the PE experiment appears to be slightly shorter (~355 days) than 1 yr. As noted in HWH, it seems reasonable to conclude that the N90L80 model has the internal dynamics to produce a QLO, but that the period of this spontaneous oscillation is close to 1 yr. Once the seasonal forcing is included in the model, the QLO locks onto the annual cycle.

The N90L80 model requires substantial computational resources, so experiments have been performed at coarser horizontal resolution. Integrations with an N30L80 version failed to produce any significant mean flow oscillation in the tropical stratosphere. However, the control model with N45L80 resolution did produce a QLO in the equatorial wind similar to that seen in the N90L80 model. The N45L80 control was initialized from a snapshot in March of the fourth year of the N90L80 seasonal run. The simulated equatorial $\overline{u}$ for the 20 yr starting in the following January (labeled here as years 1–20) are shown in Fig. 2. The results are similar to those in the N90L80 run in that a semiannual oscillation dominates in the mesosphere, but an annual oscillation with downward-propagating shear zones dominates the stratosphere. The stratospheric oscillation has a smaller amplitude in the N45 version and does not penetrate as far down into the lower stratosphere as it does in the N90 simulation. There is also a certain amount of irregularity from period to period, with the easterly phase in the lower stratosphere being almost absent in years 9, 13, and 16.

A PE version of the N45L80 model was also initialized from a snapshot of results from March of the fourth year of the N90L80 seasonal run. Results for the equatorial $\overline{u}$ over 6 yr starting in the following January are shown in Fig. 3. For the first 4 yr the results show a clear QLO with period of about 15 months. This again suggests that the N45L80 model has an unforced oscillation with period close to a year, but that the incorporation of the annual cycle tends to phase lock the equatorial oscillation (although with the irregularities in the QLO in the seasonally forced model noted above).

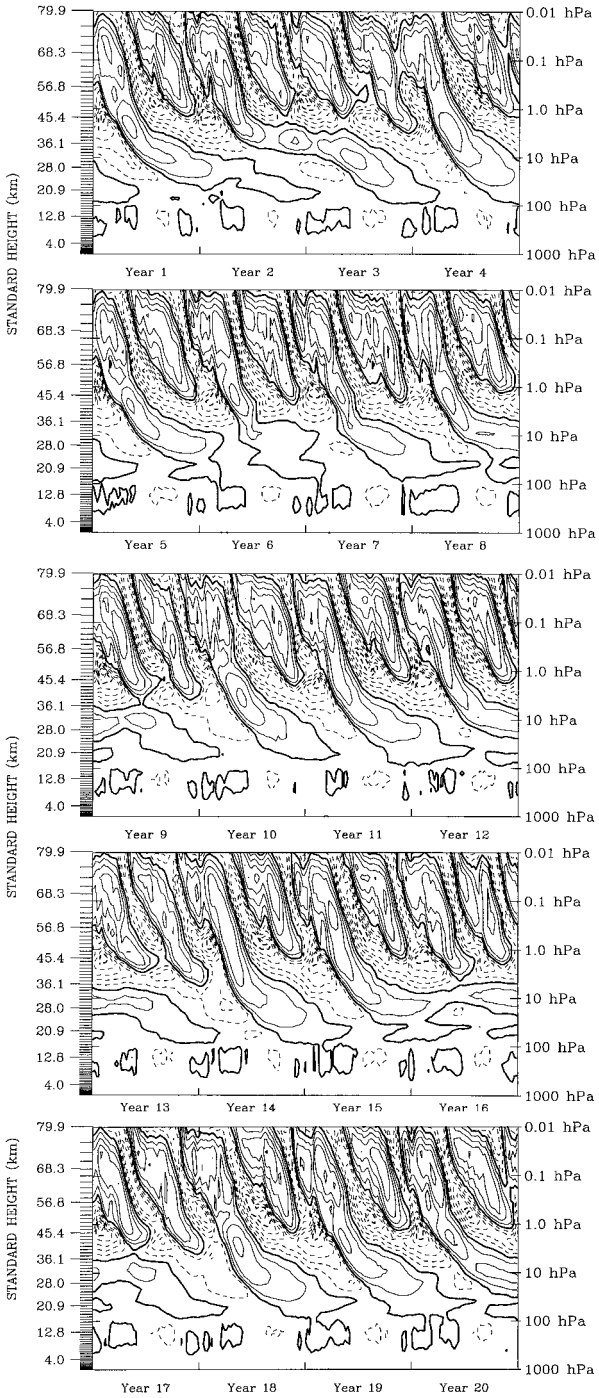

FIG. 2. As in Fig. 1 but for the seasonally varying N45L80 model integration.

The oscillation in the PE control abruptly stops near the end of year 4 and the equatorial wind structure remains rather constant, with the alternating easterly and westerly jets in the vertical still evident, but without the downward propagation. The integration has continued for over two years past the point where the oscillation stopped. It is impossible to tell for certain whether the

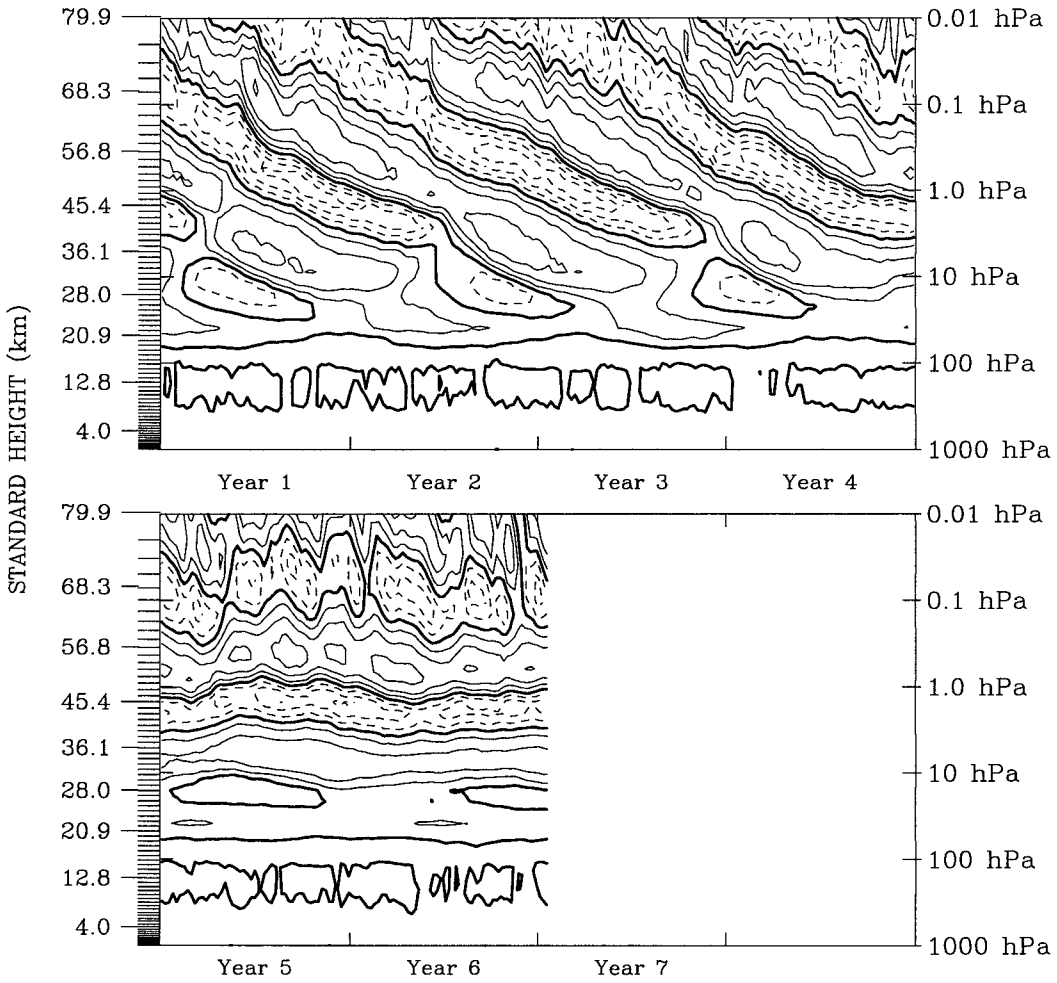

FIG. 3. As in Fig. 1 but for a perpetual equinox N45L80 integration.

downward-propagating QLO would spontaneously reappear if the integration were to be continued still further.

The tropical mean flow oscillations in both the N90L80 and N45L80 PE integrations display multiple jets stacked vertically. At any given time there are generally four or five distinct westerly or easterly jets apparent. The real QBO typically displays at most three alternating jets below the region where the semiannual oscillation becomes prominent. It is not clear how the real atmosphere would behave in the absence of the seasonal forcing, of course. The multiple jet structure in the present GCM simulations is also different from the solutions found in the simple Lindzen–Holton type models, even when generalized to multiple waves (Saravanan 1990). This contrast between the present GCM results and simpler models will be discussed in sections 5 and 7 below.

Figure 4 shows the height–latitude structure of the amplitude of the oscillation in the N90L80 and N45L80 PE runs. In each case the amplitude has been determined by a least squares fit of $\overline{u}$ at each height and latitude to a sinusoid over two full periods. The equatorial amplitude is maximized by assuming a period of about 355 days for the N90L80 run and about 475 days in the N45L80 run. The meridional modulation of the amplitude in each case is quite realistic when compared with similar harmonic analysis of the QBO in real observations (e.g., Reed 1965). In each case the meridional structure is approximately Gaussian and centered directly on the equator, with a half-width of about 12°–13° latitude. Haynes (1998) noted that the meridional scale of the real QBO may be primarily related to the latitude-dependence of the response timescale of mean flow to mechanical forcing. Haynes arguments suggest that the meridional scale of a stratospheric equatorial mean flow oscillation should be a function only of the oscillation period and the vertical scale of mean flow accelerations, and independent of the details of the mechanical driving (e.g., from waves).

The vertical structure of the amplitude does differ somewhat between the model and observations. The observed QBO amplitude rises from near zero at 100 hPa, peaks at about 25 m s^{-1} near 30 hPa, and decays slowly

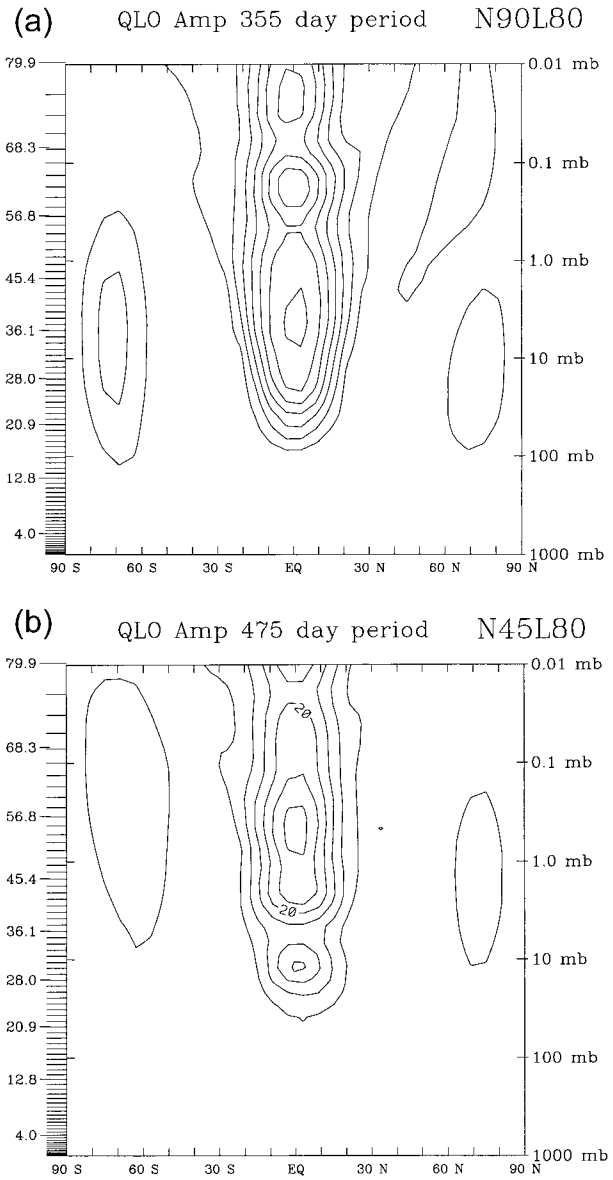

FIG. 4. Height–latitude structure of the amplitude of the QLO in the zonal-mean zonal wind, determined by a fit of a single Fourier harmonic. (top) N90L80 perpetual equinox simulation assuming a period of 355 days. (bottom) N45L80 perpetual equinox simulation assuming a period of 475 days. The contour interval is 5 m s^{-1}.

with height above 30 hPa until about 3 hPa (~40 km) when the amplitude drops fairly rapidly with height (e.g., Belmont et al. 1974; Hamilton 1981). QBO effects are found even at higher levels all the way up to the mesopause, but they appear mainly as a QBO modulation of the stronger annual and semiannual signals at these heights. By contrast, the model QLO amplitudes in Fig. 4 peak somewhat higher [10 hPa (mb) or above] and the amplitude is very roughly constant with height to the top of the model. The amplitude of the QLO in the lower stratosphere is weaker than observed in both models (but the difference is larger in the N45L80 model). This tendency for the QLO in SKYHI to be centered higher up than the real QBO is similar to results from other models reported by Takahashi (1996) and Horinouchi and Yoden (1998). The QLO in the N45L80 PE SKYHI runs also has a minimum in amplitude around 7 (mb) hPa, apparent in Fig. 4 and also in the actual time series of equatorial winds shown in Fig. 3.

An interesting aspect of the observed QBO is the clear tendency for the initial eastward accelerations to be more narrowly confined about the equator than the westward accelerations, or, equivalently, for the lower edge of the descending westerly jets to be particularly narrow (Hamilton 1984, 1985; Dunkerton and Delisi 1985). This basic aspect of the QBO is reproduced in the QLO in the N90L80 and N45L80 PE runs. Figure 5 (left) shows an instantaneous snapshot of $\overline{u}$ during the N90L80 PE run. The vertically stacked, equatorially trapped jets are apparent. The tendency for the bottom of the westerly jets to be narrow is well reproduced.

An interesting feature of the midstratospheric observations discussed in Hamilton (1984) is that the westerly equatorial jets can become narrow enough that the mean flow curvature on the flanks of the jet is very large. In the observations analyzed by Hamilton (1984) the quantity $\gamma = \beta - \overline{u}_{yy}$ was found to become negative on both flanks of the westerly jet in its initial stages. The persistence of regions of negative γ was surprising since $\gamma < 0$ is the necessary condition for barotropic instability to develop. This led Hamilton to question the accuracy of the observational analysis that he had developed (based on a simple interpolation of raw radiosonde wind data). Recently the issue of possible barotropic instability in the westerly jet flanks has been revived by Shuckburgh et al. (2001), who found that, when the wind values in the ECMWF reanalysis are used, the computed value of γ does typically drop below zero around 15°S and 15°N in the initial eastward acceleration phase of the QBO (at least near 30 hPa where they looked). Further they actually found evidence for enhanced eddy motions at these locations and times, which they attribute to the development of barotropically unstable waves. Of course, there is no guarantee that even the modern ECMWF reanalyses are reliable enough in the tropical stratosphere to accurately compute γ. Thus it is of interest to see if the present free-running GCM spontaneously simulates regions of $\gamma < 0$ in the westerly jet flanks. Figure 5 (right) shows the value of γ (normalized by β) computed from the instantaneous wind field from the N90L80 PE run shown in Fig. 4 (top). The regions of negative γ around 15°S and 15°N at the base of the westerly jet near 10 hPa are apparent. The results in this figure are quite typical of the N90L80 PE run, and the regions of negative γ are persistent features that follow the westerly jet descent (and so may exist at a single level for ~1–2 months). These GCM results support the observational studies of Hamilton (1984) and Shuckburgh et al. (2001), and may even help lend credibility to the ECMWF reanalyses in

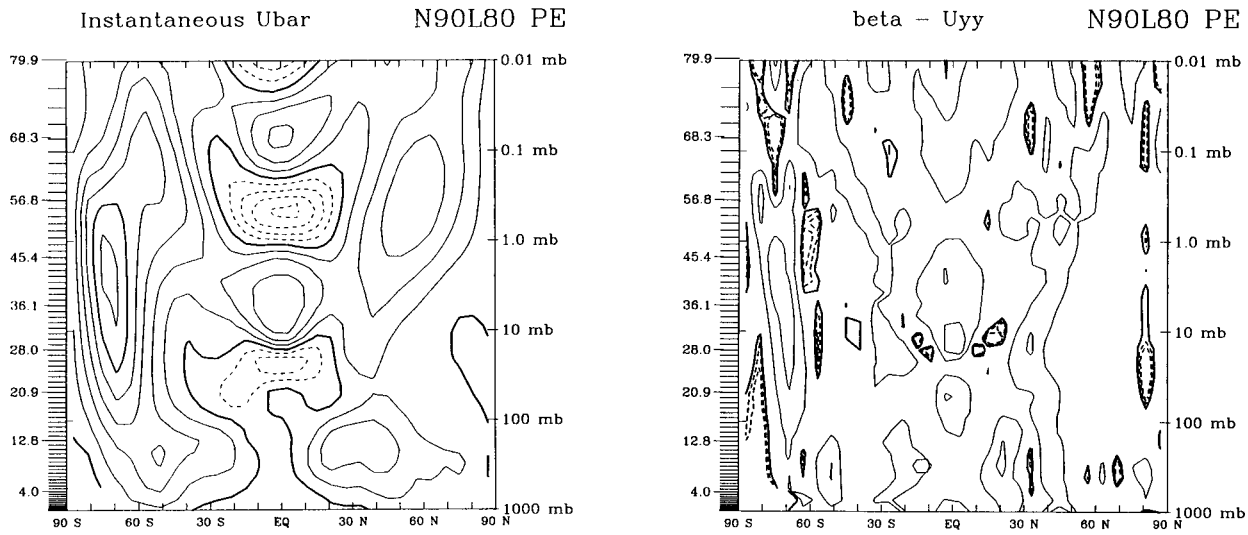

FIG. 5. (left) Instantaneous height–latitude section of the zonal-mean zonal wind from 11 Apr of year 3 of the N90L80 perpetual equinox experiment. The contour interval is 10 m s^{-1} and easterly winds are denoted by dashed contours. (right) Corresponding value of the parameter $\beta - \overline{u}_{yy}$ normalized by the equatorial value of β. The solid contours have values of 0, 1, 2, etc., while the dashed contours have one-tenth the magnitude, corresponding to values of -0.1, -0.2, etc.

the low-latitude stratosphere. The issue of the development of barotropically unstable waves in the QBO and the role that associated eddy transports may play in dynamics and trace constituent budgets will be subjects of future research using the high-resolution SKYHI model.

Figure 6 shows instantaneous cross sections of $\overline{u}$ for two times during the N45L80 PE control run, the first (Fig. 6 top) during the time when the model was still oscillating and the second (Fig. 6 bottom) near the end of the run after the mean flow oscillation had ceased. In Fig. 6 (top) the multiple stacked equatorial jets are apparent, as is the narrow lower edge of the descending westerly jet above 1 hPa (mb). The results at the later time shown in Fig. 6 (bottom) are also characterized by multiple jets, but the typical vertical shears are somewhat smaller in magnitude than during the oscillating period. The generally weaker peak equatorial vertical shears after the end of year 5 can also be seen in Fig. 3.

Figures 5 and 6 also show typical results for the winds in the extratropical middle atmosphere in the two PE control runs. There is generally a westerly jet in the extratropics of each hemisphere, with strength that varies significantly from month to month in an apparently random fashion. In the Northern Hemisphere there can even be brief periods with mean easterlies at high latitudes, a phenomenon that is analogous to the midwinter sudden warming in the real atmosphere. There is no immediately apparent connection between the extratropical and tropical zonal-mean circulation variations, although a more detailed statistical analysis might uncover some weak coupling (note the modest QLO amplitude maxima in the extratropics in Fig. 4). Notably, the character of the extratropical variability does not seem to change after year 5 when the tropical oscillation in the N45L80 PE run stops.

Finally, it should be noted that L40 versions of the model have been run with horizontal resolution as fine as N270, and none of these models show any indication of QLO behavior in the tropical stratosphere (see HWH). It appears that there is a fairly clear dividing line between the spatial resolutions that produce QLOs in SKYHI and those that do not: versions with resolution coarser than L80 in the vertical or N45 in the horizontal do not oscillate.

5. Detailed analysis of the N45L80 control simulation

This section will discuss detailed diagnosis of the dynamics of the mean flow oscillation in the N45L80 PE control run. Only results from the N45 PE control will be discussed in detail, since the same model was used in a number of additional experiments to be described and analyzed in the following section. However, the general conclusions concerning the forcing mechanisms for the QLO in the N45L80 model apply also to the N90L80 model.

The transformed-Eulerian mean (TEM) zonal-mean zonal momentum budget was diagnosed from 4-hourly snapshots of the model run. The details of TEM diagnosis for SKYHI are given in Andrews et al. (1983). In the region of the model with isobaric coordinates (i.e., pressures less than 353 hPa) the mean flow acceleration at any time step can be diagnosed exactly as the sum of forcing from (i) the Eliassen–Palm flux divergence (EPFD) associated with the eddy motions, (ii) the Coriolis torque and mean momentum advection associated

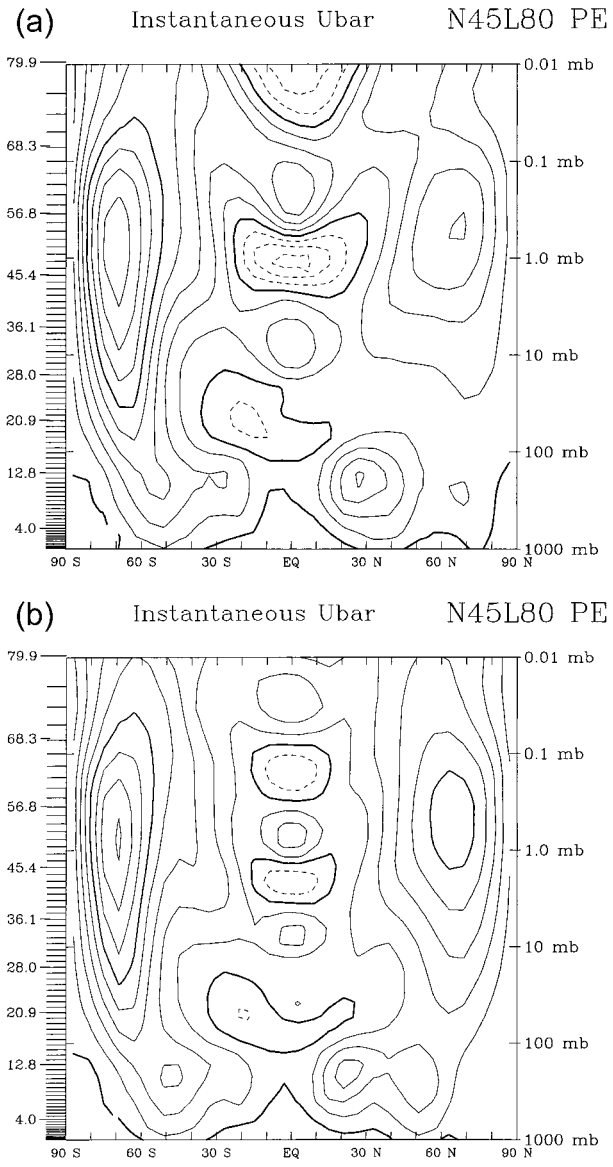

FIG. 6. Instantaneous zonal-mean zonal wind from the N45L80 perpetual equinox control run: (top) 27 Oct of year 1 and (bottom) 9 Jun of year 6. The contour interval is 10 m s^{-1} and easterly winds are denoted by dashed contours.

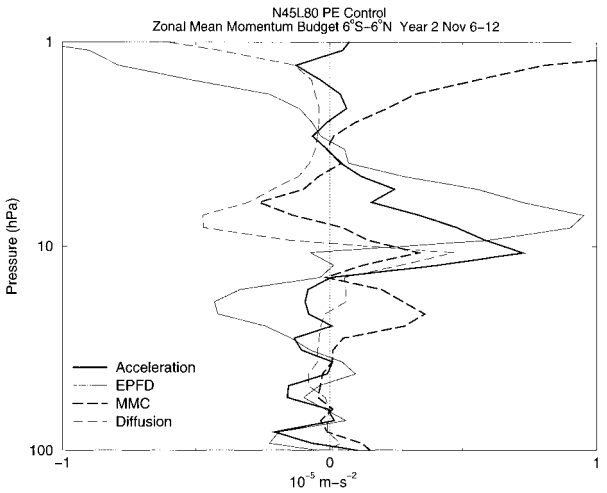

FIG. 7. Components of the zonal-mean zonal momentum budget averaged over 6°S to 6°N and over a 1-week period in Nov of year 2 of the N45L80 perpetual equinox control experiment. Terms shown are the actual mean flow acceleration, the wave driving by Eliassen–Palm flux divergence (EPFD), the momentum advection plus Coriolis torque by the transformed-Eulerian mean meridional circulation (MMC), and the subgrid-scale diffusion of momentum. Results for 100 to 1 hPa.

with the TEM mean meridional circulation, and (iii) the effects of parameterized momentum diffusion. Figure 7 shows these components of the momentum budget averaged over 6°S–6°N (i.e., the six model grid rows closest to the equator) plotted as a function of height up to 1 hPa (~50 km). The results are for a 7-day period in November of year 2 of the N45L80 PE run and thus represent an average over 42 4-hourly snapshots through that period. This finite time sampling does produce some noise in the sense that the simulation includes high-frequency zonally symmetric gravity waves that are essentially irrelevant to the rest of the circulation, but that contaminate the instantaneous (single time step) zonal-mean momentum budget [see Hamilton and Mahlman (1988) for more discussion of this issue]. Some of the small vertical scale variations seen in Fig. 7 (and budget figures to be discussed below) may be attributable to this sampling problem.

The most obvious aspect of the mean flow evolution at this time is the rapid transition from easterlies to westerlies near 10 hPa (see Fig. 3). The acceleration term in Fig. 7 does show a large positive peak near 10 hPa. This is matched by an even larger positive peak in the eddy forcing term (EPFD) that is centered slightly higher. Below about 8 hPa there is a region of negative acceleration (with some superimposed small-scale noise) that is also paralleled by a negative eddy forcing. Figure 8 shows the same components of the TEM momentum budget, but for the region above 1 hPa. At these levels as well, alternating regions of positive and negative acceleration occur near the same heights as peaks in the eddy-forcing term. The overall pattern is one in which the eddy forcing term has a banded structure in the vertical, but this term is generally opposed by the effects of the TEM mean meridional circulation and the momentum diffusion, leading to significantly smaller realized accelerations. This general picture is consistent throughout the levels and at all times during the integration. The wave driving is very largely associated with the divergence of the vertical component of the Eliassen–Palm flux as shown in Figs. 9 and 10, which compare the total EPFD with that obtained by including only the vertical component of the Eliassen–Palm flux. Thus the prime driver of the equatorial mean flow oscillation appears to be vertically propagating waves, in agreement with theoretical expectations (Lindzen and Holton 1968;

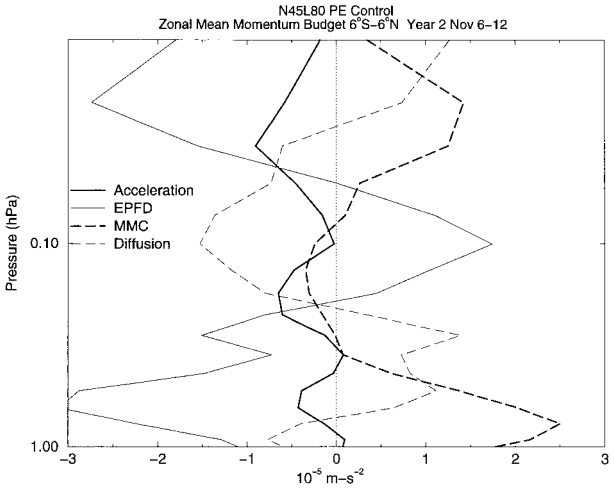

FIG. 8. As in Fig. 7 but for 1 to 0.01 hPa.

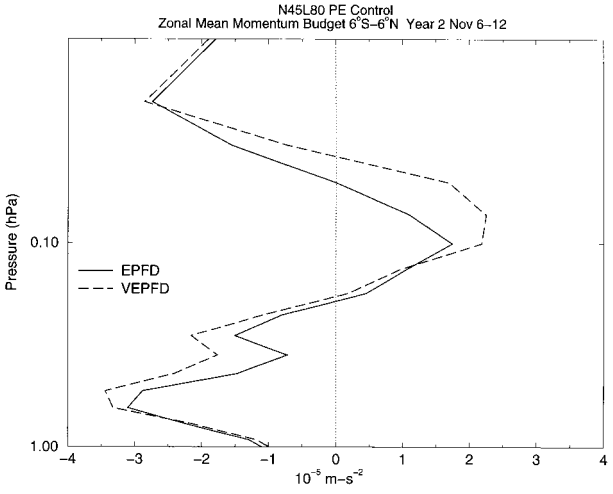

FIG. 10. As in Fig. 9 but for 1 to 0.01 hPa.

Holton and Lindzen 1972) and also with the analysis of the earlier imposed-QBO SKYHI experiment discussed by Hamilton (1998).

Figure 11 compares the forcing of the zonal-mean zonal momentum by the vertical and horizontal subgrid-scale momentum diffusion terms. The peak horizontal diffusion contribution appears considerably smaller than the peak vertical contribution, but it is not negligible. The effects of the vertical diffusion are concentrated in regions of strong mean flow shear, where the Richardson number criterion for mixing is more often satisfied. The pattern seen in Fig. 11 is again similar to that found in the earlier forced QBO experiment of Hamilton (1998).

Remarkably, the general picture of the momentum balance for the N45L80 PE control described above does not change substantially even after the QLO has ceased. Figure 12 shows the decomposition of the momentum budget for a 7-day period during June of year 5. The basic pattern of alternating layers of EPFD largely opposed by the effects of the mean meridional circulation and diffusion is also characteristic of the nonoscillating period of the integration. This momentum balance diagnosis does not, by itself, provide an explanation for why the mean flow accelerations after the end of year 4 tend to be rather random and do not persist in the organized manner that characterized the earlier period of the experiment.

The strong connection between the mean flow acceleration and the wave driving (EPFD) is demonstrated in Fig. 13, which shows height–time sections of the acceleration and EPFD terms averaged over 6°S–6°N

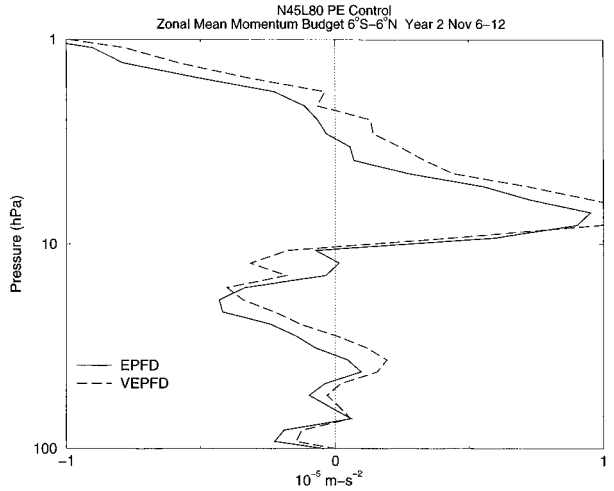

FIG. 9. Components of the zonal-mean zonal momentum budget averaged over 6°S to 6°N and over a 1-week period in Nov of year 2 of the N45L80 perpetual equinox control experiment. Shown are the total wave driving by Eliassen–Palm flux divergence (EPFD) and that from only the convergence of the vertical component of the Eliassen–Palm flux (VEPFD). Results for 100 to 1 hPa.

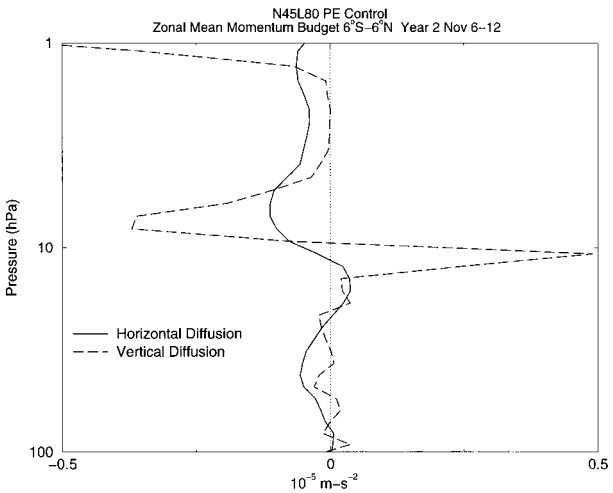

FIG. 11. Comparison of the zonal-mean momentum forcing from the vertical and horizontal components of the parameterized diffusion. Results averaged over 6°S to 6°N and over a 1-week period in Nov of year 2 of the N45L80 control perpetual equinox experiment.

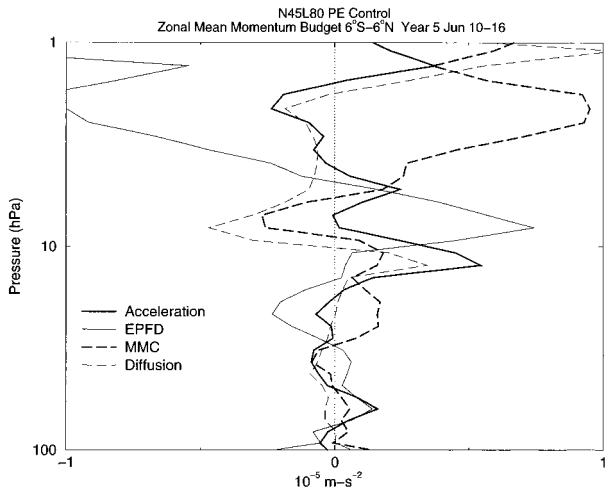

FIG. 12. As in Fig. 7 but for a week during Jun of year 5 of the N45L80 perpetual equinox control run.

for years 1–4 of the N45L80 PE control run. The downward descending zones of acceleration correspond closely with similar zones of the EPFD. Even the asymmetry between the relatively brief eastward acceleration phase and longer westward acceleration phase is reflected in the EPFD. Figure 13 is at least consistent with the view that the EPFD drives the QLO, but that the effects of EPFD are opposed by other terms, leading to realized accelerations of the same sign as the EPFD, but with substantially lower magnitude. Figure 14 shows the same quantities for years 5 and 6 when the QLO has stopped. The rather random nature of the accelerations is apparent, and there no longer seems to be any clear correlation between the EPFD and mean flow accelerations. However, the EPFD does maintain a banded vertical structure as in the earlier part of the run, but now without systematic downward propagation. The banded structure of EPFD presumably reflects the in-

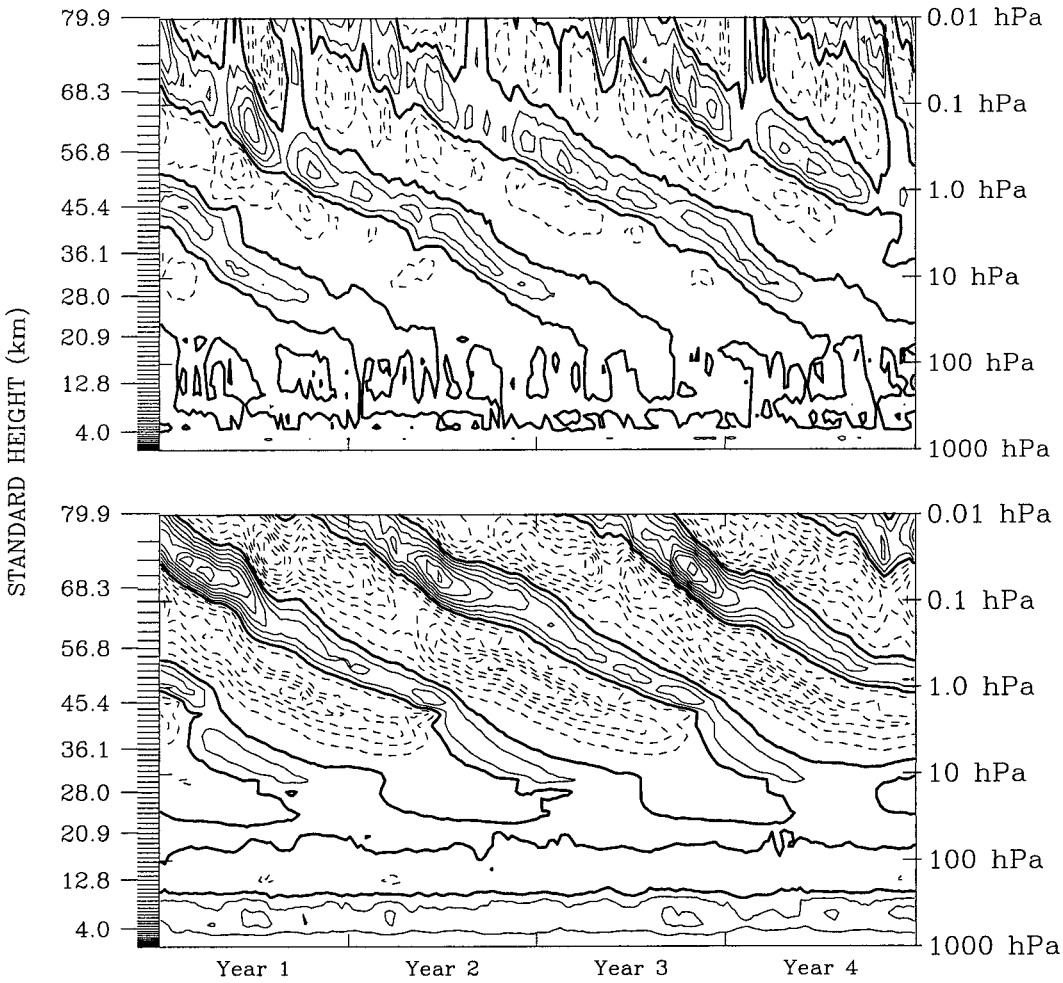

FIG. 13. Time–height section of components of the zonal-mean zonal momentum budget averaged over 6°S to 6°N for years 2–5 of the N45L80 perpetual equinox control run. (top) The actual mean flow acceleration. Contour interval is 0.25×10^{-5} m s^{-2} and westward accelerations are denoted by dashed contours. (bottom) The total wave driving by Eliassen–Palm flux divergence. Contour interval is 0.5×10^{-5} m s^{-2} and westward forcing is denoted by dashed contours. The quantities plotted are running means over 49 days.

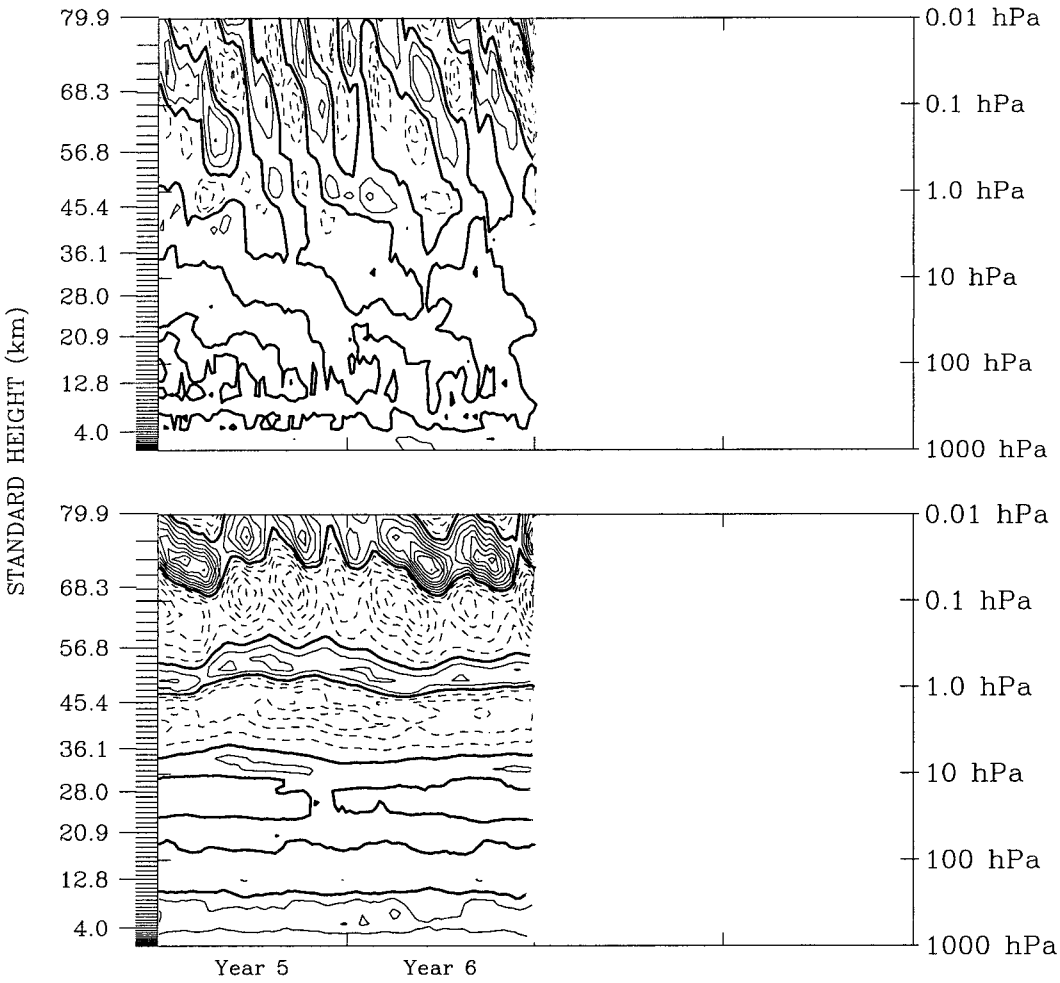

FIG. 14. As in Fig. 13 but for years 5 and 6 of the N45L80 perpetual equinox control run.

fluence of the mean flow and mean flow shear on wave absorption. In the nonoscillating phase of the integration, the wave forcing can continue to maintain the alternating jets, but it is not strong enough to lead to the oscillatory QBO-like behavior seen earlier.

The data for several 40-day segments in the N45L80 PE control was subject to space–time Fourier analysis using the procedure of Hayashi (1971). This decomposes each variable into eastward- and westward-propagating components with different wavenumbers and frequencies. Figure 15 shows the vertical eddy momentum flux F averaged over 6°S–6°N and divided into eastward- and westward-propagating components, F_E and F_W, during November–December of year 2. Here F is defined as $-\overline{u'\omega'}$, where the overbar denotes a zonal average, the prime a deviation from the zonal average, and ω is the usual vertical velocity in isobaric coordinates. The sign convention is such that $F > 0$ corresponds to an upward flux of positive (eastward) zonal momentum. Figure 15 shows that both F_E and F_W decay with height over most altitudes, but that the decay rate varies strongly with altitude. Figure 15 also shows the near-equatorial mean flow averaged over the same 40-day period. The strong westerly jet between 10 and 1 hPa is accompanied by a sharp drop in eastward flux and only a very small decrease in the westward flux, consistent with the expectations from Eqs. (1) and (2). This analysis was repeated for a total of five 40-day segments during the N45L80 PE control (see Table 1), which included both the oscillating and nonoscillating periods of the integration. Figure 16 shows F_E and F_W computed for period 1 during the oscillating phase and for period 5, long after the mean flow oscillation had stopped. The fluxes up to about 80 hPa are very similar in the two segments, suggesting that the change in mean flow behavior after the end of year 4 is not due to any significant change in the wave fluxes emerging from the tropical troposphere. Flux profiles above 80 hPa are very different in the two segments, but this presumably reflects the different stratospheric mean flows at these two times.

Figure 17 shows the contributions to F_E and F_W from various zonal wavenumber ranges. The resolved model spectrum extends to zonal wavenumber 75, but the eddy

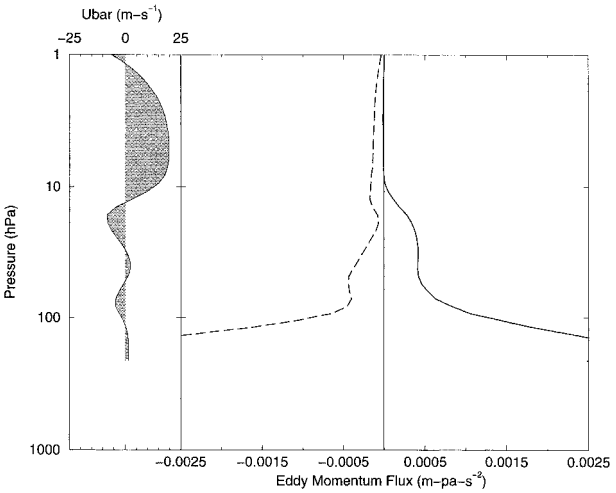

FIG. 15. (right) The upward flux of zonal momentum by all eddies averaged between 6°S and 6°N resolved into eastward- (solid) and westward- (dashed) propagating waves. Results for the 40-day period number 1 in the N45L80 perpetual equinox control run. (left) The equatorial zonal-mean zonal wind for the same period.

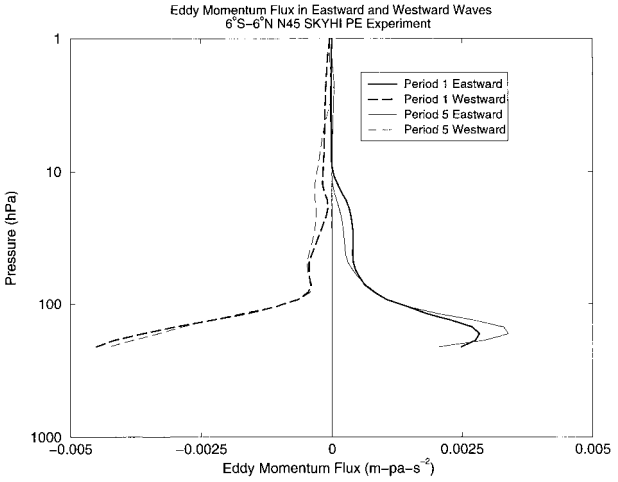

FIG. 16. The upward flux of zonal momentum by all eddies averaged between 6°S and 6°N resolved into eastward- (solid) and westward- (dashed) propagating waves for two periods during the N45L80 perpetual equinox control run.

momentum flux is largely (>90%) concentrated in the first half of this wavenumber range (i.e., waves with wavelength at least four times the grid spacing), consistent with earlier analyses of various versions of SKYHI (e.g., Miyahara et al. 1986; Hamilton and Mahlman 1988; Hayashi et al. 1989). Figure 17 shows that within this first half of the wavenumber range the fluxes are rather broadly distributed—certainly there is no particular dominance by the planetary-scale waves.

Figure 18 shows the eddy flux F partitioned by zonal phase speed for period 1 of the N45L80 PE control at levels from 104 hPa (~18 km) to 6.98 hPa (~35 km). There is a general tendency for waves with $(c - \overline{u})$ greater than (less than) zero to make positive (negative) contributions to F, consistent with theoretical results for linear, steady waves with predominantly upward propagation. Near the tropopause (104 hPa) the flux is concentrated in waves with phase speeds less than about 30 m s^{-1}. At higher levels the range of phase speeds with substantial contributions to F becomes broader. This is consistent with the enhanced attenuation of flux expected for waves with small $|(c - \overline{u})|$ [Eqs. (1) and (2)]. The relative enhancement of westward relative to eastward waves at 6.98 hPa where the mean flow becomes strongly westerly is also apparent. Figure 19 shows the same quantities but for levels from 3.33 hPa (~40 km) to 0.05 hPa (~70 km). The general pattern of a broader spectrum of phase speeds at higher altitudes is seen here as well. In fact, at the highest levels there are significant fluxes even at $|(c - \overline{u})|$ of 100 m s^{-1} or more. These waves will not come close to critical levels but may break nonlinearly. Certainly in the extratropical mesosphere, there has been clear evidence in the SKYHI model of gravity wave drag produced by breaking gravity waves with very large Doppler-shifted

TABLE 1. The 40-day segments chosen for intensive analysis in various N45L80 perpetual equinox integrations.

PE control period 1—2 Nov–11 Dec, year 2
PE control period 2—25 May–3 Jul, year 3
PE control period 3—1 Sep–10 Oct, year 4
PE control period 4—4 Nov–13 Dec, year 4
PE control period 5—1 Nov–10 Dec, year 6
Warm SST period 1—1 Jul–9 Aug, year 2
Warm SST period 2—4 Aug–12 Sep, year 4
Cool SST—1 Jul–9 Aug, year 2
Enhanced horizontal diffusion—2 Jun–11 Jul, year 3

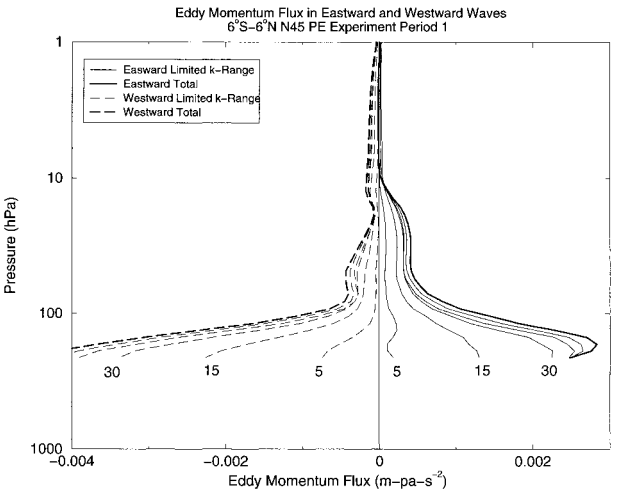

FIG. 17. The upward flux of zonal momentum by all eddies averaged between 6°S and 6°N resolved into eastward- (heavy solid) and westward- (heavy dashed) propagating waves during period 1 of the N45L80 perpetual equinox control run. Also shown are the fluxes associated with ranges of zonal wavenumber 1–5, 1–15, 1–30, 1–45, and 1–60 (light solid and dashed lines). (Lines for 1–45 and 1–60 are not labelled).

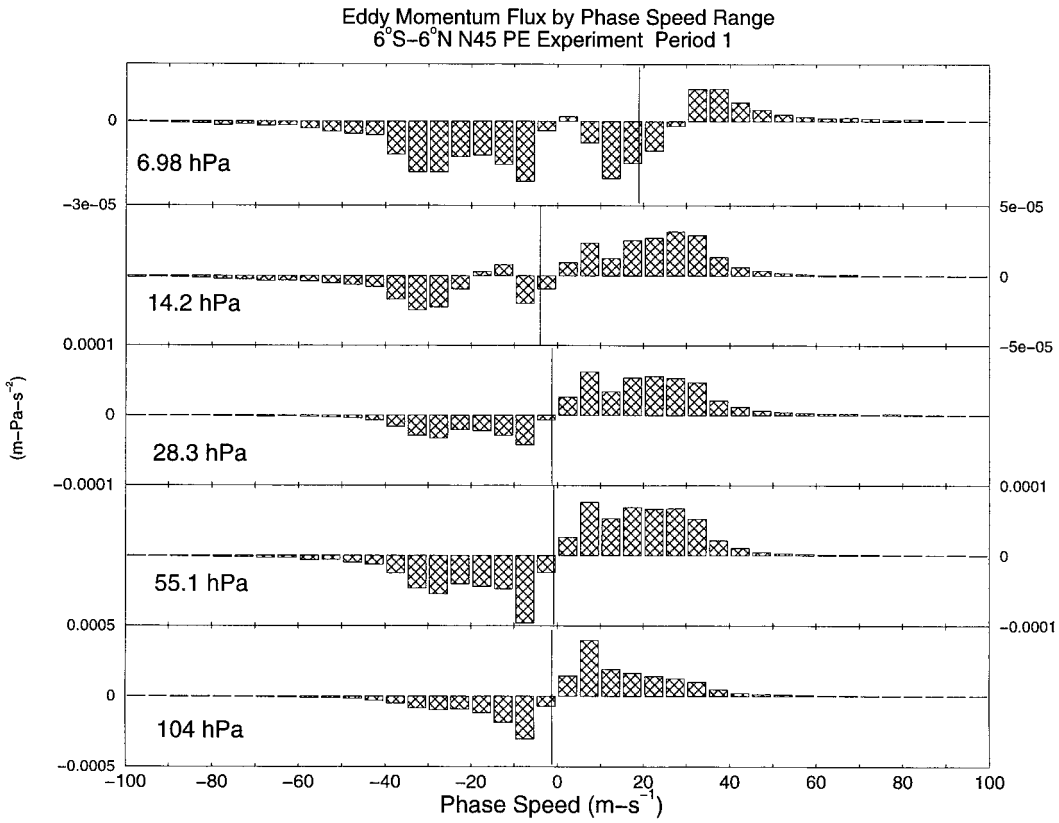

FIG. 18. The upward flux of zonal momentum by all eddies averaged between 6°S and 6°N partitioned by zonal phase speed at different pressure levels. Results for the period 2 Nov–11 Dec year 2 of the N45L80 perpetual equinox control run. Note that the vertical scale is different for each panel and the labels on vertical scale for each panel alternate between the right and left sides. The vertical lines mark the mean zonal wind values for this period at each level.

phase speeds (e.g., Miyahara et al. 1986; Hayashi et al. 1989).

Figures 18 and 19 provide evidence that the wave spectrum in the full GCM is controlled by more complex processes than the simple steady propagation and absorption embodied in Eqs. (1) and (2). Note that if the wave field is upward propagating and the waves and mean flow are both steady, then the sign of F associated with any horizontal phase speed should be the same as that of $(c - \overline{u})$. The local 40-day mean $\overline{u}$ is shown at each level in Figs. 18 and 19. Below about 7 hPa the theoretical expectation for the sign of F is borne out by the spectral analysis, but at higher levels it is violated for some ranges of c. The implication is that the unsteadiness of the waves or mean flow is important, and/or that there is significant downward-propagating wave activity in some phase speed intervals. Secondary wave generation in the model as the primary (tropospherically generated) waves break in the upper stratosphere and mesosphere is a possibility and could help account for some of the complicated nature of the phase speed spectra of F at high levels.

The top two panels of Fig. 20 show the phase speed spectrum of F near the tropopause for two 40-day segments during the control PE run: period 1 (see Table 1) during the oscillating phase of the experiment, and period 5 near the end of the run when the mean flow oscillation had ceased. The spectra of waves emerging from the tropical tropopause are very similar in the two segments, suggesting once again that changes in tropospheric wave generation are not responsible for the sudden change in mean flow behavior in the PE control run.

6. Perturbed N45L80 simulations

A number of additional integrations were performed with modified versions of the N45L80 PE model. One set of runs was designed to help understand the nature of the transition from nonoscillating behavior to QLO behavior when the model resolution is increased. One reasonable hypothesis would be that at sufficiently low resolution the SKYHI horizontal and vertical subgrid-scale diffusions might be large enough to suppress the equatorial mean-flow oscillations.

In the enhanced horizontal diffusion (EHD) experi-

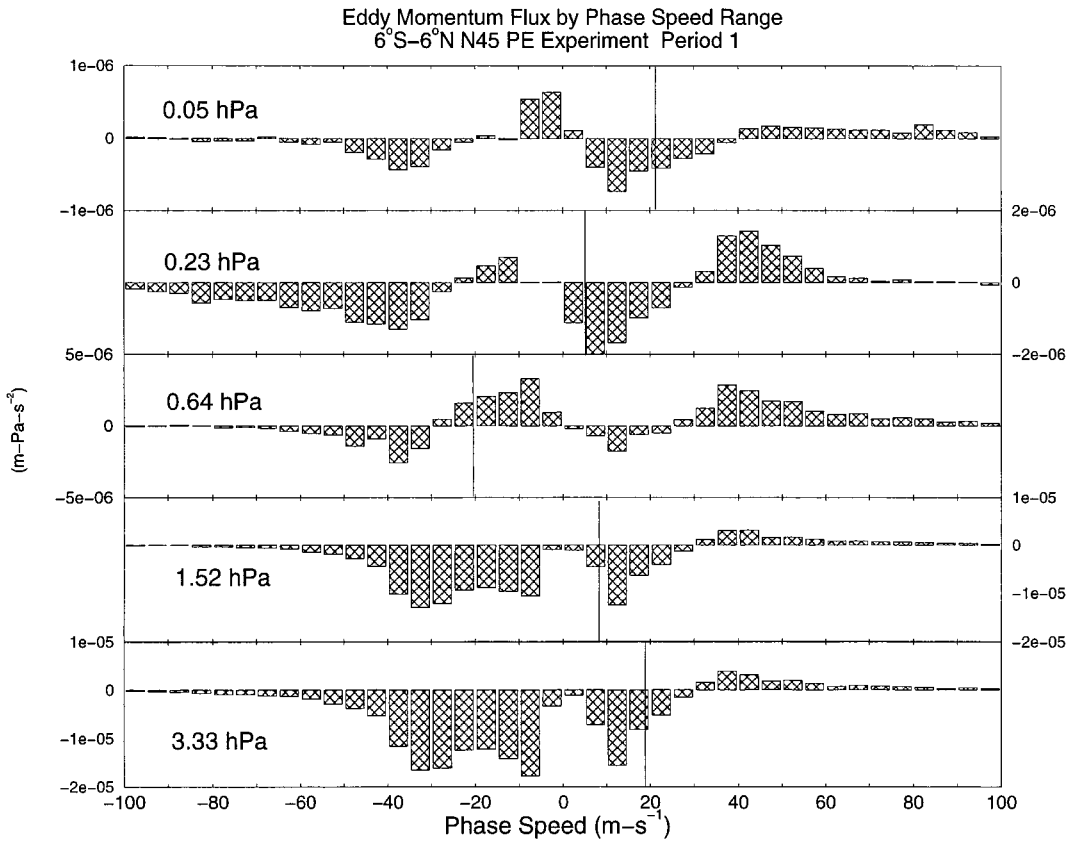

FIG. 19. As in Fig. 18 but for higher levels.

ments, the horizontal diffusion coefficient (for both momentum and heat) in the N45L80 PE run was increased to the value appropriate for N30 resolution [i.e., the coefficient was multiplied by $(3/2)^2$]. The result for the equatorial $\overline{u}$ evolution in the first EHD run is displayed in Fig. 21 (top). This figure shows the control N45L80 PE experiment results to 6 March of year 3 at which point the horizontal diffusion was increased to the N30 value. Almost immediately the downward-propagating mean flow oscillation ceased, and the QLO did not reappear in the following ~2 yr of integration. Figure 21 (bottom) shows the results for a second EHD run in which the diffusion was enhanced on 9 March of year 4 of the control. Again the downward progression of mean wind reversals is suppressed immediately. It seems reasonable to conclude that the enhanced horizontal diffusion prevents the development of a QLO, and that this may explain why versions of SKYHI with N30 (or coarser) horizontal resolution do not simulate a QLO in the equatorial circulation. Unfortunately, the inverse of this experiment, that is, running N30 SKYHI with horizontal diffusion reduced to the N45 value, is not possible as the standard horizontal diffusion coefficients used in SKYHI are needed to maintain numerical stability. Any substantial reduction (>25%) of the standard values leads to blowup of the solution.

The enhanced horizontal diffusion in these experiments could affect the equatorial stratospheric zonal-mean circulation in at least two ways. One would simply be through its direct effect on the zonal-mean momentum balance, while another would be through changing the upward-propagating wave fluxes emerging into the stratosphere. Figure 22 shows the equatorial eddy momentum fluxes F_E and F_W in the upper troposphere and lower stratosphere during five 40-day segments of the control experiment (see Table 1) and for one 40-day segment of the first EHD experiment. The fluxes in the EHD run do appear to be somewhat (~5%–10%) smaller than those in the control near the tropopause (near 104 hPa), but this is unlikely to explain the lack of a QLO in the EHD run (a much more dramatic reduction in flux is found in another experiment with reduced SSTs discussed below, and this greater reduction does not suppress the QLO in that version of the model). Figure 20 (bottom panel) shows the zonal phase speed spectrum of the eddy momentum flux at 104 hPa in the EHD experiment, and this looks quite similar to the results for the control experiment (Fig. 20 top two panels).

In the enhanced vertical diffusion (EVD) experiment, the vertical diffusion in the N45L80 model was replaced by values appropriate for the L40 level structure, that is, the Δz factors in Eq. (7) were essentially doubled

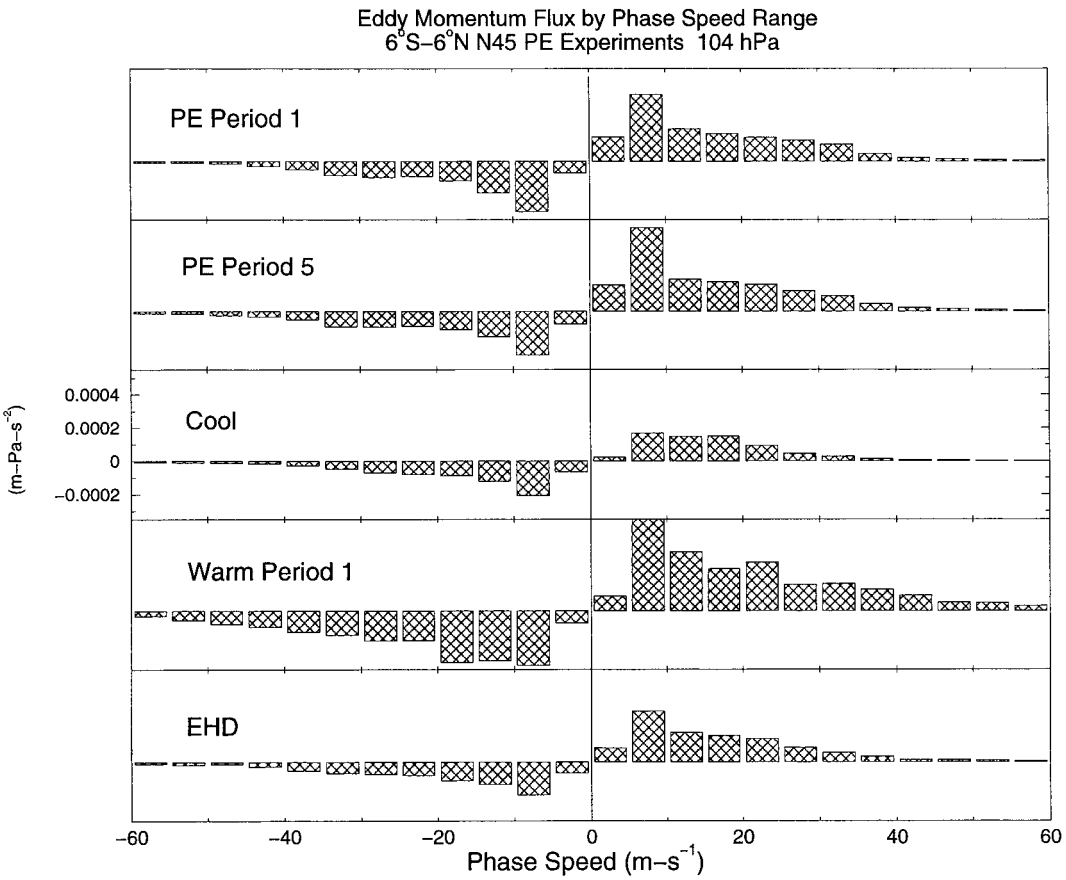

FIG. 20. The upward flux of zonal momentum at 104 hPa by all eddies averaged between 6°S and 6°N, partitioned by zonal phase speed. Results for 40-day segments from different experiments. Period 1 in the N45L80 perpetual equinox control run, period 5 in the N45L80 perpetual equinox control run, the cool SST N45L80 experiment, period 1 in the warm SST N45L80 experiment, and the first enhanced horizontal diffusion N45L80 experiment. See Table 1 for the limits of the special 40-day analysis periods.

from their L80 values. Figure 23 shows the equatorial mean wind evolution in the same format as in Fig. 21 (top), that is, the N45L80 control results are shown till 6 March of year 3 when the EVD was applied. The effect of the EVD is very much less dramatic than for the EHD, and the QLO continues with similar amplitude and period for the remaining ~3 yr of the integration. This is convincing evidence that requirement of fine vertical resolution for simulation of a QLO in SKYHI arises from some other reason than the concomitant reduction in the vertical diffusion. Close inspection of Fig. 23 does show that the EVD has a subtle effect on the mean flow evolution, with a slight reduction in the peak shears in the equatorial $\overline{u}$ field after the EVD is applied.

Two additional experiments were performed with the N45L80 PE model. In one the prescribed SSTs were raised over that in the control by $2.5(1 + \cos\theta)$ °C, and in the other they were reduced by the same amount, where θ is the latitude. These integrations were initialized from the N45L80 PE control experiment results on 4 March of year 1. The large perturbations to the SSTs produced noticeable changes in the tropospheric circulations, and, in particular, the warm (cool) SST run had enhanced (reduced) low-latitude precipitation. This is shown in Fig. 24, which displays the zonal-mean precipitation rates calculated over two 40-day periods in the control, and in the warm and cool SST runs. Figure 25 shows the results for the equatorial $\overline{u}$ for the warm and cool experiments. Initially both experiments display clear QLOs, but with the cool SST case having a longer period (~510 days) than the control, and the warm SST case having a shorter period (~350 days) than the control. This is consistent with the expectation based on simple theory outlined in section 2—warmer SSTs lead to stronger wave forcing that should result in a shorter period for the stratospheric mean flow oscillation. The enhancement of the wave fluxes with increasing SSTs has itself been documented. For example, Fig. 26 shows the equatorial momentum fluxes F_E and F_W for the warm SST experiment compared with those in the control, while Fig. 27 shows the same comparison between the cool SST case and the control. The zonal

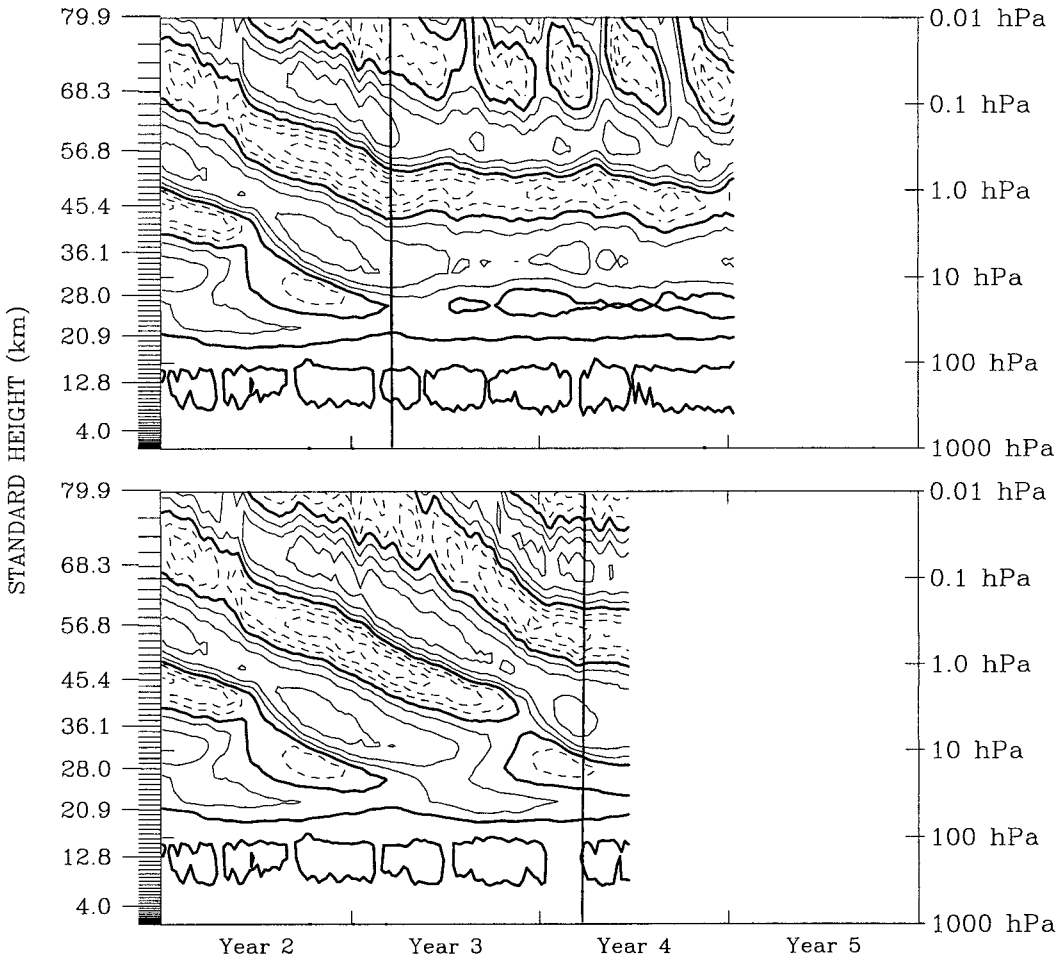

FIG. 21. Time–height section of the equatorial zonal-mean zonal wind in (top) the first N45L80 enhanced horizontal diffusion experiment with the enhancement imposed on 6 Mar of year 3 and (bottom) the second N45L80 enhanced horizontal diffusion experiment with enhancement imposed on 9 Mar of year 4. The vertical lines mark the time of introduction of the enhanced diffusion in each case. The contour interval is 10 m s^{-1} and dashed contours denote easterly winds.

phase speed spectra of the eddy momentum flux at 104 hPa for the warm and cool SST cases are displayed together with that from samples of the control run in Fig. 20. The enhanced (reduced) fluxes in the warm SST case are quite apparent.

The cool SST integration has been continued through the end of year 7 (not shown) and the QLO continues in a similar fashion as in years 2–5. As seen in Fig. 25 (top), the warm SST integration has an abrupt transition to a nonoscillating state at the end of year 3, and the oscillation is not reestablished in the following 14 months of the run. This shift to a nonoscillating state is presumably analogous to what happened at the end of year 4 of the N45L80 PE control.

Except for the transition to a nonoscillating state in the warm case, the behavior of the period of the stratospheric equatorial $\overline{u}$ oscillation in the perturbed SST runs is consistent with expectations. These experiments represent a rather direct demonstration of the close coupling of the tropical stratospheric mean flow evolution with tropospheric convection.

7. Discussion and conclusions

The GFDL SKYHI model can display large amplitude, long period oscillations of the mean flow in the tropical stratosphere when run with sufficiently fine vertical and horizontal resolution. The simulated mean flow oscillation has a peak amplitude, meridional structure, and vertical propagation that are all similar to those characteristic of the observed QBO. However, in all cases considered the model oscillation has a period that is very roughly half of that of the real QBO, making this a ''QBO-like'' oscillation in the terminology of Takahashi (1996). When seasonal forcing is included, the QLO in SKYHI tends to lock strongly onto the annual

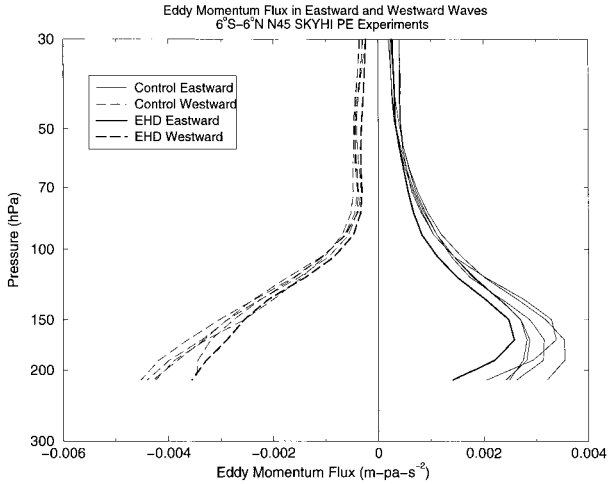

FIG. 22. The upward flux of zonal momentum by all eddies averaged between 6°S and 6°N resolved into eastward (solid) and westward (dashed) propagating waves for five 40-day periods (light lines) during the N45L80 perpetual equinox control run and during a 40-day period during the enhanced horizontal diffusion experiment (heavy lines).

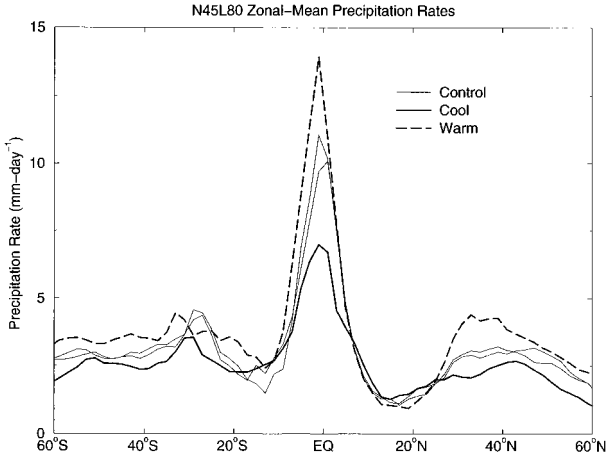

FIG. 24. Zonal-mean precipitation rates in two 40-day segments of the N45L80 perpetual equinox control run, and in 40-day segments of the warm SST and cool SST N45L80 simulations.

period, so the emphasis here has been on the simpler case of perpetual equinox simulation. In PE mode the model appears to display two distinct regimes for tropical mean wind behavior. When initialized from a seasonally varying version (as all the control PE integrations reported here have been), or from a snapshot from an oscillating PE run (as in the present perturbed PE integrations), the various model versions appear immediately to simulate a fairly regular tropical mean flow oscillation. In two of the runs considered here (control N45L80 PE and N45L80 warm SST), after a few cycles the oscillation spontaneously and abruptly stops, leaving a state characterized by alternating easterly and westerly mean flow jets, but no persistently descending shear zones characteristic of the oscillating phase.

The meridional structure of the SKYHI-simulated QLO is remarkable in reproducing the very narrow initial eastward mean flow accelerations that have been reported in the available observational studies of the QBO. In fact, the model at high resolution (N90L80) produces mean westerly jets so narrow that the necessary criterion for barotropic instability is regularly satisfied on both flanks (around 15° latitude). This feature has also been seen in observational analyses, but the limited accuracy of such analyses in the tropical stratosphere could lead to reasonable doubt about the validity of this finding. The present model result, that is, that regions of strong mean flow curvature can spontaneously develop and persist on the flanks of the descending

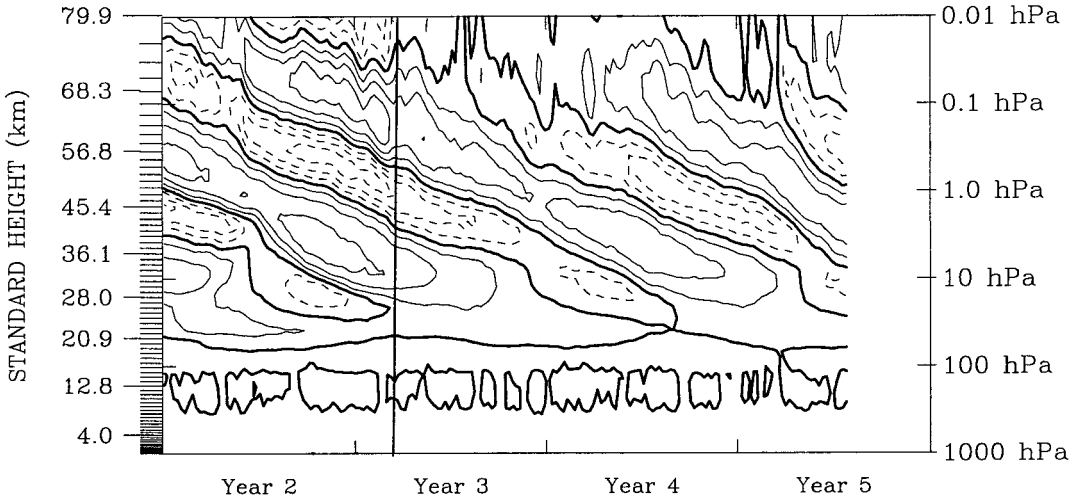

FIG. 23. Time–height section of the equatorial zonal-mean zonal wind in the N45L80 enhanced vertical diffusion experiment. The vertical line marks 6 Mar of year 3 when the enhanced diffusion coefficient was imposed. The contour interval is 10 m s^{-1} and dashed contours denote easterly winds.

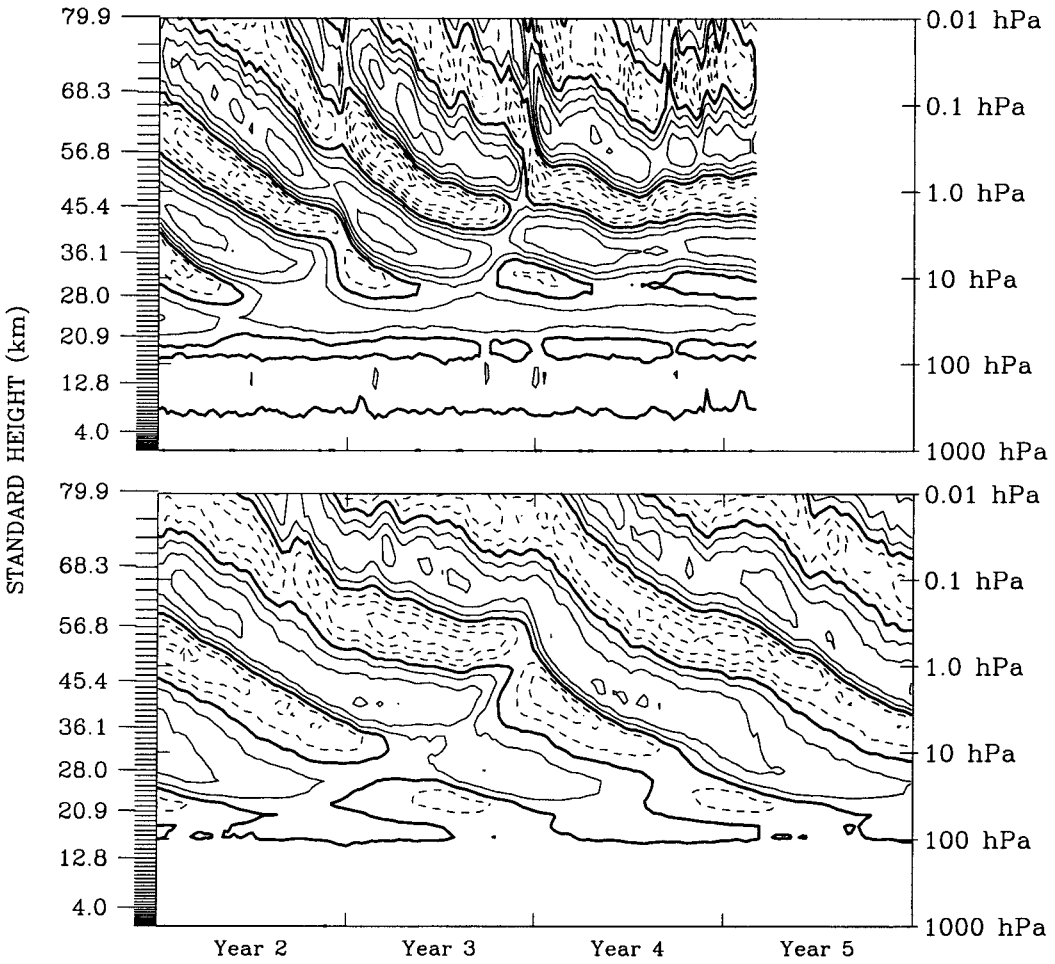

FIG. 25. Time–height section of the equatorial zonal-mean zonal wind in (top) the N45L80 warm SST experiment, and (bottom) the N45L80 cool SST experiment. The contour interval is 10 m s^{-1} and dashed contours denote easterly winds.

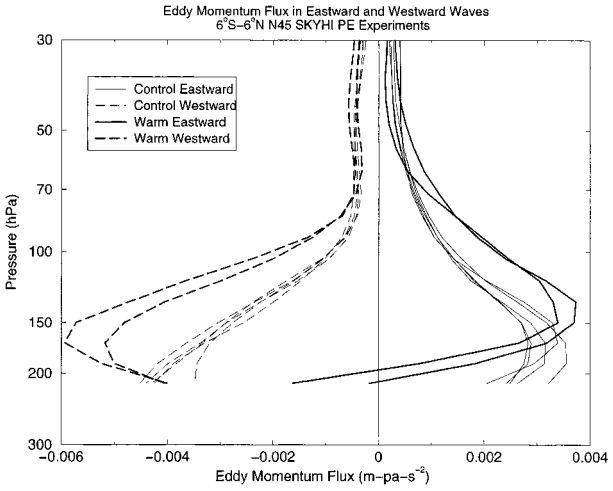

FIG. 26. The upward flux of zonal momentum by all eddies averaged between 6°S and 6°N resolved into eastward- (solid) and westward- (dashed) propagating waves for five 40-day periods during the N45L80 perpetual equinox control run (light lines) and during two 40-day periods during the warm SST experiment (heavy lines).

westerly jet, actually lends credibility to the observational analyses in the tropical stratosphere.

A detailed study of the zonal-mean zonal momentum balance in the tropical stratosphere in the PE control run reveals a fairly clear pattern. The mean flow accelerations are largely forced by mean flow driving associated with vertically propagating waves, but generally are opposed by the effects of mean flow advection and subgrid-scale momentum diffusion. As noted by Dunkerton (1997) the estimated observed mean upwelling in the tropical stratosphere is comparable in magnitude to the QBO descent rates, and this means that the vertical mean advection of zonal momentum should play an important role in opposing the accelerations that cause the descent of the QBO. Thus it is not surprising that a similar opposition is seen in the present model results. The effects of both the horizontal and vertical subgrid scale viscosity are also significant and typically also oppose the wave forcing. The net result is that the wave forcing needed to make the model oscillate is perhaps approximately three times that of the

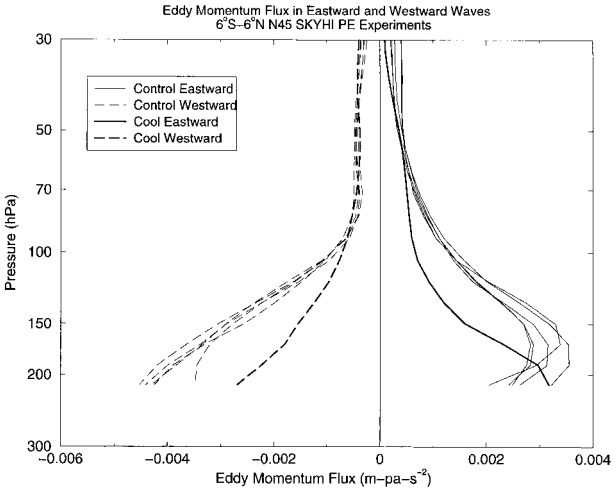

FIG. 27. The upward flux of zonal momentum by all eddies averaged between 6°S and 6°N resolved into eastward (solid) and westward (dashed) propagating waves for five 40-day periods during the N45L80 perpetual equinox control run (light lines) and during a 40-day period during the cool SST experiment (heavy lines).

realized accelerations in the oscillation. These results on the zonal-mean zonal momentum budget are very similar to those seen in the earlier SKYHI study of Hamilton (1998) with an imposed tropical QBO.

The vertically propagating waves that are responsible for forcing the QLO in SKYHI appear to have a rather broad distribution in horizontal scales and phase speeds. In this regard the present GCM behavior is closer to that of Horinouchi and Yoden (1998) and Takahashi (1999), who also found a broad spectrum of waves involved in their model QLO, than to that of Takahashi (1996), who found that planetary-scale waves accounted for most of the mean flow driving of the QLO in his model. It also makes the behavior of the SKYHI GCM more analogous to the idealized continuous spectrum model of Lindzen and Holton (1968) model than to the discrete wave models of Holton and Lindzen (1972) or Plumb (1977).

There are two aspects of the present simulations that are surprising, particularly in light of the behavior of the simple idealized models such as Lindzen and Holton (1968) and Holton and Lindzen (1972). One is the spontaneous cessation of the oscillation in two of the PE runs. This seems to occur in the absence of any obvious change in the upward flux of waves or in the behavior of the extratropical stratospheric flow. A plausible speculation for this is that at some random point in the mean flow evolution, the peak vertical shears in the tropical middle atmosphere become somewhat reduced. Since the wave forcing in the Lindzen–Holton limit is proportional to the mean flow shear, it may simply be that given the somewhat weaker mean shears to work with, the wave driving is never again strong enough to restore the larger earlier peak shears. The behavior here may be somewhat analogous to that of the Lindzen–Holton model itself, for which an extra source of shear (assumed in their case to be associated with the semiannual oscillation) needed to be included to begin the wave–mean flow interaction that led to their mean flow oscillation. It is interesting that in the seasonally forced SKYHI runs, the strong equatorial mean flow oscillation never ceases (at least during 20 yr of N45L80 control and over 4 yr of N90L80 control). Perhaps including the seasonal cycle ensures that there is always another source of mean flow shear at low latitudes in addition to the vertical wave–mean flow interaction itself.

The other surprising aspect of the QLO in the PE runs is the presence of several vertically stacked easterly and westerly jets in the tropical middle atmosphere. This would not happen in the simplest mechanistic models of the QBO. For example, in the Holton–Lindzen (1972) model, the presence of a jet of one sign virtually eliminates the further vertical propagation of wave flux associated with the wave with phase speed of the same sign, preventing any formation of jets of the same sign farther aloft. The present GCM appears to differ from the simple QBO models in at least two important ways. One is that the horizontal phase speed spectrum in the tropical middle atmosphere in the model can become quite broad at high altitudes, and the other is that the waves may be dissipated nonlinearly, even at levels where $|(c - \overline{u})|$ is large. Thus mean flow accelerations forced in the stratosphere may be caused by strong wave absorption near critical levels, and at higher altitudes by nonlinear breaking of much faster waves. It is interesting that the mechanistic two-dimensional model of Mayr et al. (1997) does also display multiple descending equatorial jets. The wave forcing in their case is provided by the gravity wave drag parameterization of Hines (1997). The Hines parameterization attempts to represent an extended continuous spectrum in horizontal phase speed, and also includes nonlinear saturation mechanisms for the parameterized waves.

Perturbation experiments were conducted with the GCM to test the sensitivity to subgrid-scale diffusion. In one set of experiments the horizontal diffusion coefficient in the N45L80 model was increased to that normally used in the N30 versions of the model. This immediately caused the mean flow oscillation to cease, strongly suggesting that the reason that SKYHI needs fine horizontal resolution to simulate a QLO is the concomitant reduction in subgrid-scale horizontal viscosity. These results are consistent with Plumb's (1984) speculation that relatively coarse resolution GCMs (and particularly the SKYHI model) do not simulate a QBO because of excessive horizontal viscosity. A similar experiment with the vertical diffusion produced exactly the opposite result. Specifically, increasing the vertical diffusion in the N45L80 model to that normally used in the L40 versions (which do not oscillate) had minimal effect on the tropical QLO.

Experiments were also conducted with rather large

global perturbations introduced into the SST field. These had the effect of changing the precipitation field in the Tropics, which in turn greatly affected the flux of waves emerging into the tropical stratosphere. This provided a GCM analogue of the experiments reported by Plumb (1977), in which he varied the amplitude of the wave fluxes in a simple idealized two-wave QBO model. The present GCM simulations are consistent with Plumb's earlier results in the sense that increased (decreased) convection and wave fluxes lead to a shortening (lengthening) of the QLO period. This is a fairly direct demonstration of the coupling between tropospheric convection and stratospheric mean flow behavior, at least in the GCM context.

Acknowledgments. The authors thank Jerry Mahlman for helpful discussions and for his long-term support for this work.

REFERENCES

Andrews, D. G., J. D. Mahlman, and R. W. Sinclair, 1983: Eliassen–Palm diagnostics of wave-mean flow interaction in the GFDL SKYHI general circulation model. *J. Atmos. Sci.,* **40,** 2768–2784.

Belmont, A. D., D. G. Dartt, and G. D. Nastrom, 1974: Periodic variations in stratospheric zonal wind from 20 to 65 km at 80°N to 70°S. *Quart. J. Roy. Meteor. Soc.,* **100,** 203–211.

Cariolle, D., M. Amodei, M. Deque, J.-F. Mahfouf, P. Simon, and H. Teyssedre, 1993: A quasi-biennial signal in general circulation model simulations. *Science,* **261,** 1313–1316.

Dunkerton, T. J., 1997: The role of gravity waves in the quasibiennial oscillation. *J. Geophys. Res.,* **102,** 26 053–26 076.

——, and D. Delisi, 1985: Climatology of the equatorial lower stratosphere. *J. Atmos. Sci.,* **42,** 1199–1208.

Fels, S. B., J. D. Mahlman, M. D. Schwarzkopf, and R. W. Sinclair, 1980: Stratospheric sensitivity to perturbations in ozone and carbon dioxide: Radiative and dynamical responses. *J. Atmos. Sci.,* **37,** 2265–2297.

Hamilton, K., 1981: The vertical structure of the quasi-biennial oscillation: Observations and theory. *Atmos.–Ocean,* **19,** 236–250.

——, 1984: Mean wind evolution through the quasi-biennial cycle in the tropical lower stratosphere. *J. Atmos. Sci.,* **41,** 2113–2125.

——, 1985: The initial westerly acceleration phase of the stratospheric quasi-biennial oscillation as revealed in FGGE analyses. *Atmos.–Ocean,* **23,** 188–192.

——, 1996: Comprehensive meteorological modelling of the middle atmosphere: A tutorial review. *J. Atmos. Terr. Phys.,* **58,** 1591–1628.

——, 1998: Effects of an imposed quasi-biennial oscillation in a comprehensive troposphere–stratosphere–mesosphere general circulation model. *J. Atmos. Sci.,* **55,** 2393–2418.

——, and J. D. Mahlman, 1988: General circulation model simulation of the semiannual oscillation in the tropical middle atmosphere. *J. Atmos. Sci.,* **45,** 3212–3235.

——, and L. Yuan, 1992: Experiments on tropical stratospheric mean wind variations in a spectral general circulation model. *J. Atmos. Sci.,* **49,** 2464–2483.

——, R. J. Wilson, J. D. Mahlman, and L. J. Umscheid, 1995: Climatology of the SKYHI troposphere–stratosphere–mesosphere general circulation model. *J. Atmos. Sci.,* **52,** 5–43.

——, ——, and R. Hemler, 1999: Middle atmosphere simulated with high vertical and horizontal resolution versions of a GCM: Improvement in the cold pole bias and generation of a QBO-like oscillation in the Tropics. *J. Atmos. Sci.,* **56,** 3829–3846.

Hayashi, Y., 1971: A generalized method of resolving disturbances into progressive and retrogressive waves by space Fourier and time cross-spectral analysis. *J. Meteor. Soc. Japan,* **49,** 125–128.

——, 1974: Spectral analysis of tropical disturbances appearing in a GFDL general circulation model. *J. Atmos. Sci.,* **31,** 180–218.

——, D. G. Golder, J. D. Mahlman, and S. Miyahara, 1989: The effect of horizontal resolution on gravity waves simulated by the GFDL SKYHI general circulation model. *Pure Appl. Geophys.,* **130,** 421–443.

Haynes, P. H., 1998: The latitudinal structure of the quasi-biennial oscillation. *Quart. J. Roy. Meteor. Soc.,* **124,** 2645–2670.

Hines, C. O., 1997: Doppler-spread parameterization of gravity-wave momentum deposition in the middle atmosphere. Part I: Basic formulation. *J. Atmos. Solar-Terr. Phys.,* **59,** 371–386.

Holton, J. R., and R. S. Lindzen, 1972: An updated theory for the quasi-biennial cycle of the tropical stratosphere. *J. Atmos. Sci.,* **29,** 1076–1080.

Horinouchi, T., and S. Yoden, 1998: Wave-mean flow interaction associated with a QBO-like oscillation simulated in a simplified GCM. *J. Atmos. Sci.,* **55,** 502–526.

Kasahara, A., and T. Sasamori, 1974: Simulation experiments with a 12-layer stratospheric global circulation model. II. Momentum balance and energetics in the stratosphere. *J. Atmos. Sci.,* **31,** 408–421.

Levy, H., J. D. Mahlman, and W. J. Moxim, 1982: Tropospheric N_2O variability. *J. Geophys. Res.,* **87,** 3061–3080.

Lindzen, R. S., 1971: Equatorial planetary waves in shear: Part I. *J. Atmos. Sci.,* **28,** 609–622.

——, and J. R. Holton, 1968: A theory of the quasi-biennial oscillation. *J. Atmos. Sci.,* **25,** 1095–1107.

Mahlman, J. D., and R. S. Sinclair, 1980: Recent results from the GFDL troposphere–stratosphere–mesosphere general circulation model. *Proc. ICMUA Sessions at IUGG Symp. 18*, 11–18.

Manabe, S., and B. G. Hunt, 1968: Experiments with a stratospheric general circulation model. I: Radiative and dynamical aspects. *Mon. Wea. Rev.,* **96,** 477–502.

——, and J. D. Mahlman, 1976: Simulation of seasonal and interhemispheric variations in the stratospheric circulation. *J. Atmos. Sci.,* **33,** 2185–2217.

Mayr, H. G., J. G. Mengel, C. O. Hines, K. L. Chan, N. F. Arnold, C. A. Reddy, and H. S. Porter, 1997: The gravity wave Doppler spread theory applied in a numerical spectral model of the middle atmosphere. Part 2: Equatorial oscillations. *J. Geophys. Res.,* **102,** 26 093–26 015.

Miyahara, S., Y. Hayashi, and J. D. Mahlman, 1986: Interaction of gravity waves and planetary scale flow simulated by the GFDL SKYHI general circulation model. *J. Atmos. Sci.,* **43,** 1844–1861.

Pawson, S., and Coauthors, 2000: The GCM-reality intercomparison for SPARC: Scientific issues and initial results. *Bull. Amer. Meteor. Soc.,* **81,** 781–796.

Plumb, R. A., 1977: The interaction of two internal waves with the mean flow: Implications for the theory of the quasi-biennial oscillation. *J. Atmos. Sci.,* **34,** 1847–1858.

——, 1984: The quasi-biennial oscillation. *Dynamics of the Middle Atmosphere,* J. R. Holton and T. Matsuno, Eds., Terra Scientific Publishing, 217–251.

——, and A. D. McEwan, 1978: The instability of a forced standing wave in a viscous stratified fluid: A laboratory analogue of the quasi-biennial oscillation. *J. Atmos. Sci.,* **35,** 1827–1839.

Reed, R. J., 1965: The present status of the 26-month oscillation. *Bull. Amer. Meteor. Soc.,* **46,** 374–386.

Saravanan, R., 1990: A multiwave model of the quasi-biennial oscillation. *J. Atmos. Sci.,* **47,** 2465–2474.

Sato, K., and T. J. Dunkerton, 1997: Estimates of momentum flux associated with equatorial Kelvin and gravity waves. *J. Geophys. Res.,* **102,** 26 247–26 261.

Shuckburgh, E., W. Norton, A. Iwi, and P. Haynes, 2001: The influence of the quasi-biennial oscillation on isentropic transport and mixing in the Tropics and subtropics. *J. Geophys. Res.,* **106,** 14 327–14 338.

Takahashi, M., 1996: Simulation of the stratospheric quasi-biennial oscillation using a general circulation model. *Geophys. Res. Lett.,* **23,** 661–664.

——, 1999: The first realistic simulation of the stratospheric quasi-biennial oscillation in a general circulation model. *Geophys. Res. Lett.,* **26,** 1307–1310.

Tsay, C. Y., 1974: Analysis of large-scale wave disturbances in the Tropics simulated by an NCAR global circulation model. *J. Atmos. Sci.,* **31,** 330–339.

Untch, A., 1998: A simulation of the quasi-biennial oscillation with the ECMWF model. Research Activities in Atmospheric and Oceanic Modeling, WMO, 6.26–6.27.